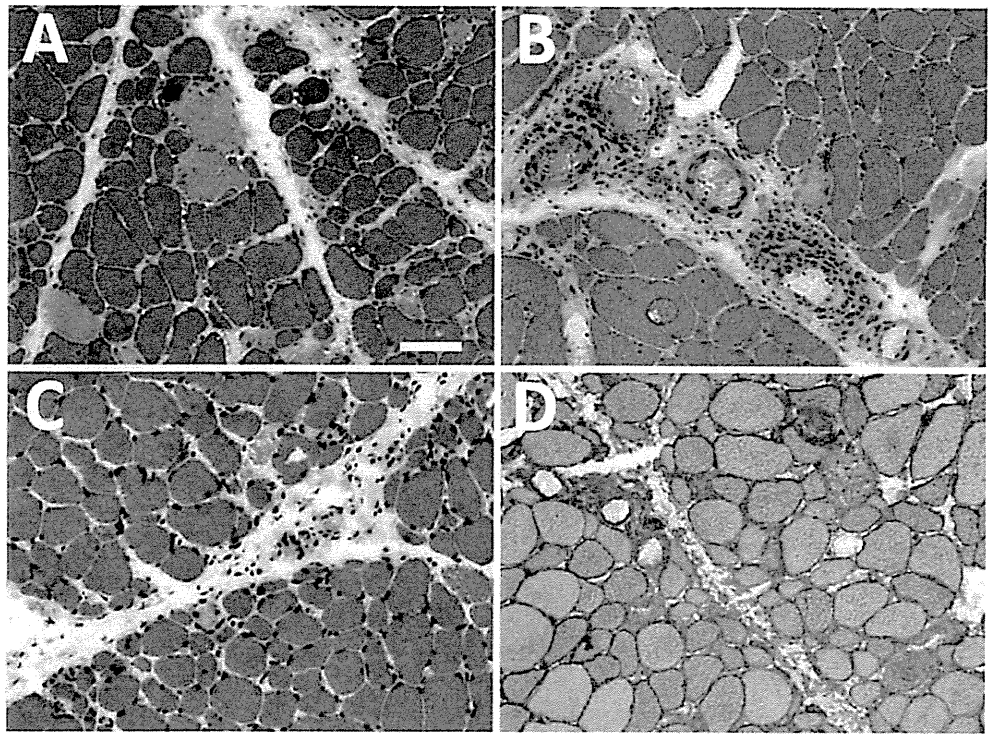

Figure 2. **Light microscopic findings of femoral muscle specimens (A-D). A biopsy of the femoral muscle showed many necrotic and regenerative fibers (A). Marked perivascular lymphocytic inflammations were found in perimysial tissue (B). Perifascicular muscle fiber atrophy was seen (C). Immunohistochemical staining for MHC class I antigens showed intense labeling of the sarcolemma of all fibers and internal labeling of perifascicular atrophic fibers (D). *Bars* A-D 100 μm. A-C, Hematoxylin and Eosin staining; D, immunohistochemical staining for MHC class I antigens.**

is frequently associated with ILD (2). Anti-Jo-1 antibody was reported in 20-30% of patients with PM/DM. ILD was more common than myositis in the early phase of disease and seemed to be one predictor of outcomes. The onset of weakness in patients with anti-Jo-1 antibody frequently occurs between the months of February and July (8). In contrast, anti-SRP antibody is clinically associated with pure PM and is found in 4-6% of patients with PM/DM (1, 3), although three patients with DM were reported among 23 Japanese patients with myositis associated with anti-SRP antibody (9). Patients with anti-SRP antibody most often present with severe muscle involvement characterized by rapidly developing proximal weakness, culminating in severe disability; the response to steroid therapy is often poor. Peculiar histopathological features include prominent muscle fiber necrosis without clinically significant inflammatory cell infiltration.

The present patient's condition was characterized by the coexistence of anti-Jo-1 antibody and anti-SRP antibody. Because the coexistence of these MSAs is associated with the clinical features of both antibodies, interacting in a complex fashion, affected patients may show more severe signs and symptoms. Another characteristic of our patient was the presence of massive pleural effusion associated with ILD. Although lung involvement is often found in patients with PM/DM, massive pleural effusion is very rare (10). The pathomechanism of the massive pleural effusion is unknown, but in this case it may have involved the exacerbation of pleural inflammation in association with pleural microvasculopathy in DM.

In conclusion, our findings strongly suggest that the coexistence of anti-Jo-1 and anti-SRP antibodies may lead to more severe clinical symptoms, including massive pleural effusion, thus expanding the clinical spectrum of idiopathic inflammatory myopathy. However, further clinical and pathological studies of similar cases are needed to establish firm conclusions.

The authors state that they have no Conflict of Interest (COI).

Contributions: K. Sugie was responsible for the overall study design, participated in the organization, planning, and coordination of the study, and wrote the manuscript. Y Tonomura and S Ueno contributed to running the study and analyzed and interpreted the data.

References

1. Targoff IN. Autoantibodies and their significance in myositis. Curr

Rheumatol Rep 10: 333-340, 2008.
2. Schmidt WA, Wetzel W, Friedländer R, et al. Clinical and serological aspects of patients with anti-Jo-1 antibodies - an evolving spectrum of disease manifestations. Clin Rheumatol 19: 371-377, 2000.
3. Miller T, Al-Lozi MT, Lopate G, Pestronk A. Myopathy with antibodies to the signal recognition particle: clinical and pathological features. J Neurol Neurosurg Psychiatry 73: 420-428, 2002.
4. Vincze M, Molnár PA, Tumpek J, et al. An unusual association: anti-Jo-1 and anti-SRP antibodies in the serum of a patient with polymyositis. Clin Rheumatol 29: 811-814, 2010.
5. Emslie-Smith AM, Arahata K, Engel AG. Major histocompatibility complex class I antigen expression, immunolocalization of interferon subtypes, and T cell-mediated cytotoxicity in myopathies. Hum Pathol 20: 224-231, 1989.
6. Emslie-Smith AM, Engel AG. Necrotizing myopathy with pipestem capillaries, microvascular deposition of the complement membrane attack complex (MAC), and minimal cellular infiltration. Neurology 41: 936-939, 1991.
7. Váncsa A, Gergely L, Ponyi A, et al. Myositis-specific and myositis-associated antibodies in overlap myositis in comparison to primary dermatopolymyositis: Relevance for clinical classification: retrospective study of 169 patients. Joint Bone Spine 77: 125-130, 2010.
8. Leff RL, Burgess SH, Miller FW, et al. Distinct seasonal patterns in the onset of adult idiopathic inflammatory myopathy in patients with anti-Jo-1 and anti-signal recognition particle autoantibodies. Arthritis Rheum 34: 1391-1396, 1991.
9. Takada T, Hirakata M, Suwa A, et al. Clinical and histopathological features of myopathies in Japanese patients with anti-SRP autoantibodies. Mod Rheumatol 19: 156-164, 2009.
10. Miyata M, Fukaya E, Takagi T, et al. Two patients with polymyositis and dermatomyositis complicated with massive pleural effusion. Intern Med 37: 1058-1063, 1998.

Available online at www.sciencedirect.com

SciVerse ScienceDirect

Neuromuscular Disorders 23 (2013) 269–276

www.elsevier.com/locate/nmd

DNAJB6 myopathy in an Asian cohort and cytoplasmic/nuclear inclusions

Takatoshi Sato [a,d], Yukiko K. Hayashi [a,b,*], Yasushi Oya [c], Tomoyoshi Kondo [e], Kazuma Sugie [f], Daita Kaneda [g], Hideki Houzen [h], Ichiro Yabe [i], Hidenao Sasaki [i], Satoru Noguchi [a,b], Ikuya Nonaka [a], Makiko Osawa [d], Ichizo Nishino [a,b]

[a] *Department of Neuromuscular Research, National Institute of Neuroscience, National Center of Neurology and Psychiatry, 4-1-1 Ogawahigashi-cho, Kodaira, Tokyo 187-8502, Japan*

[b] *Department of Clinical Development, Translational Medical Center, National Center of Neurology and Psychiatry, 4-1-1 Ogawahigashi-cho, Kodaira, Tokyo 187-8502, Japan*

[c] *Department of Neurology, National Center Hospital of Neurology and Psychiatry, 4-1-1 Ogawahigashi-cho, Kodaira, Tokyo 187-8551, Japan*

[d] *Department of Pediatrics, Tokyo Women's Medical University, School of Medicine, 8-1 Kawadacho, Shinjuku-ku, Tokyo 162-8666, Japan*

[e] *Department of Neurology, Wakayama Medical University, 811-1 Kimiidera, Wakayama 641-8509, Japan*

[f] *Department of Neurology, Nara Medical University School of Medicine, 840 Shijo-cho, Kashihara, Nara 634-8521, Japan*

[g] *Department of Neurology, Osaka Red Cross Hospital, 5-30 Fudegasaki-cho, Tenouji-ku, Osaka 543-855, Japan*

[h] *Department of Neurology, Hokkaido P.W.F.A.C. Obihiro-Kosei General Hospital, 8-1 Nishi 6-jo Minami, Obihiro 080-0016, Hokkaido, Japan*

[i] *Department of Neurology, Hokkaido University, Kita 15-jo Nishi 7, Kita-ku, Sapporo 060-8638, Hokkaido, Japan*

Received 22 October 2012; received in revised form 26 December 2012; accepted 29 December 2012

Abstract

DNAJB6, which encodes DnaJ homolog, subfamily B, member 6 (DNAJB6) was recently identified as a causative gene for limb-girdle muscular dystrophy type 1D (LGMD1D). DNAJB6 is a member of heat shock protein 40 and contains a J domain, G/F domain and C-terminal domain. Only three different mutations have been identified in 11 families. In this study, we identified seven Japanese individuals from four unrelated families who carried a *DNAJB6* mutation. We found a novel p.Phe96Ile substitution and a previously reported p.Phe96Leu change in the G/F domain of DNAJB6. All affected individuals showed slowly progressive muscle weakness, mainly in their legs, and their muscle pathology showed cytoplasmic inclusions and rimmed vacuoles. Our immunohistochemical analysis detected cytoplasmic accumulations associated with chaperone-assisted selective autophagy together with intranuclear accumulations of DNAJB6 and heat shock 22-kD protein 8 (HSPB8). This is the first report of Asian patients with LGMD1D. Our new findings may contribute to understanding the pathological mechanisms of this myopathy.

Keywords: Chaperone-assisted selective autophagy (CASA); DnaJ homolog, Subfamily B; Member 6 (DNAJB6); Heat shock protein (HSP); Protein aggregation; Limb-girdle muscular dystrophy type 1D (LGMD1D)

1. Introduction

Limb girdle muscular dystrophy (LGMD) is a form of muscular dystrophy that is clinically characterised by proximal dominant muscle weakness and atrophy. LGMD is genetically heterogeneous and classified into two major categories: autosomal dominant LGMD type 1 and autosomal recessive LGMD type 2. Over 10 years ago, four Finnish families were reported with LGMD type 1D (LGMD1D), which was linked to chromosome 7q36 and the affected individuals exhibited slow progressive muscle weakness, mainly in the lower limbs [1]. Their muscle pathology was characterised by the

* Corresponding author at: Department of Neuromuscular Research, National Institute of Neuroscience, National Center of Neurology and Psychiatry, 4-1-1 Ogawahigashi-cho, Kodaira, Tokyo 187-8502, Japan. Tel.: +81 42 341 2711x5113; fax: +81 42 346 1742.

E-mail address: hayasi_y@ncnp.go.jp (Y.K. Hayashi).

0960-8966/$ - see front matter © 2013 Elsevier B.V. All rights reserved.
http://dx.doi.org/10.1016/j.nmd.2012.12.010

presence of cytoplasmic inclusions (CIs) and rimmed vacuoles (RVs) [1]. *DnaJ homolog, subfamily B, member 6* (*DNAJB6*) was recently identified as the causative gene for the autosomal dominant form of muscular dystrophy (DNAJB6 myopathy) [2,3]. Most individuals with the *DNAJB6* mutation including the original Finnish LGMD1D family had the LGMD phenotype, although distal dominant muscle involvement was also reported [2,3]. Only three different mutations of p.Phe89Ile, p.Phe93Leu and p.Pro96Arg have been identified in 11 unrelated European and American families [2,3]. DNAJB6 contains three domains, i.e. N-terminal J domain, G/F domain and C-terminal domain, and all three mutations are located in the G/F domain [2,3]. DNAJB6 encodes two isoforms: DNAJB6a and 6b. DNAJB6a is located in the nucleus, whereas 6b, a shorter isoform, is present in both the cytosol and the nucleus [4]. A previous report suggested that only DNAJB6b is associated with the pathogenesis of this disease in the zebrafish model [3]. DNAJB6 is a member of heat shock protein 40 (HSP40) and is reported to have a role as a cardiomyocyte growth regulator [5]. Recently, DNAJB6 was also reported to suppress protein aggregation and the toxicity of disease-associated polyglutamine [4].

In this study, we confirmed the presence of individuals with LGMD1D in an Asian cohort. We screened our muscle repository and found four unrelated Japanese families who carried *DNAJB6* mutations, including a novel mutation. All of the affected individuals had the LGMD phenotype with characteristic muscle involvement. In the analysis of muscle pathology, the nuclei were a major focus because DNAJB6 is localised in the nuclei. Thus, we report the first Asian families with LGMD1D and novel nuclear findings related to their muscle pathology.

2. Patients and methods

All the clinical materials used in this study were obtained for diagnostic purposes with written informed consent. All experiments performed in this study were approved by the Ethical Committee of the National Center of Neurology and Psychiatry (NCNP).

2.1. Patients

From the NCNP muscle repository, we selected 103 cases of LGMD due to unknown causes and 89 myopathy patients with RVs or CIs in their muscle biopsies.

2.2. Muscle samples

Muscle samples were taken from biceps brachii, quadriceps femoris or gastrocnemius muscles. All samples were frozen with isopentane cooled in liquid nitrogen.

2.3. Histochemistry

Serial frozen sections of 10 μm were stained using a set of histochemical methods including hematoxylin and eosin (HE), modified Gomori trichrome (mGt), NADH-tetrazolium reductase (NADH-TR), toluidine blue, cytochrome c oxidase (COX) and actomyosin adenosine triphosphatase (ATPase pH 10.4, 4.6 and 4.2).

2.4. Immunohistochemistry

Immunohistochemistry was performed using 6 μm-thick serial frozen sections fixed in 4% paraformaldehyde for 10 min using standard protocols. The primary antibodies used in this study were as follows: anti-DNAJB6 antibody (Abnova, 1:100), anti-transactivation response DNA-binding protein (TDP-43; Protein Tech Group Inc., 1:100), anti-BCL2-associated athanogene 3 (BAG3; Abcam, 1:100), anti-heat shock 22-kDa protein 8 (HSPB8; Abcam, 1:100), anti-heat shock 70-kDa protein 8 (HSPA8; StressGen, 1:50), anti-STIP1 homology and U-box containing protein 1, E3 ubiquitin protein ligase (STUB1; Calbiochem, 1:100) and anti-lamin A/C (Chemicon, 1:100). After incubation with primary antibodies, the sections were stained using the avidin–biotin–peroxidase complex method (Vector Laboratories, Burlingame) or fluorescence-labelled secondary antibodies (Life Technologies). The sections were observed by a BX51 (Olympus, Tokyo, Japan) or an Axiophoto2 microscope (Carl Zeiss, Oberkochen, Germany) and LSM710 (Carl Zeiss, Oberkochen, Germany) with epifluorescence.

2.5. Electron microscopy

Frozen muscle sections were fixed in 2.5% glutaraldehyde and post-fixed with 2% osmium tetroxide. Semi-thin sections were stained with toluidine blue and examined by light microscopy. Ultrastructural analysis was conducted on ultrathin sections of muscles stained with uranyl acetate and lead citrate, using a transmission electron microscope (JEM 1400; Jeol, Tokyo, Japan).

2.6. Genetic analysis

Genomic DNA was isolated from muscle specimens or peripheral lymphocytes using standard techniques. All exons and the flanking intronic regions of *DNAJB6* were sequenced directly using an ABI PRISM 3130 automated sequencer (PE Applied Biosystems). The primer sequences used in this study are available on request.

3. Results

3.1. Mutation analysis of DNAJB6

We identified one novel heterozygous and one reported missense mutation in seven patients from four unrelated

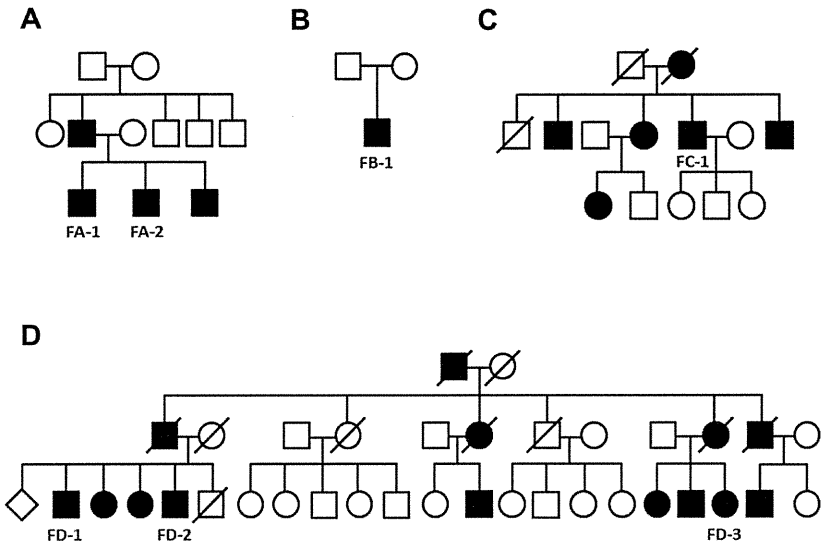

Fig. 1. Pedigree structures of families A, B, C and D.

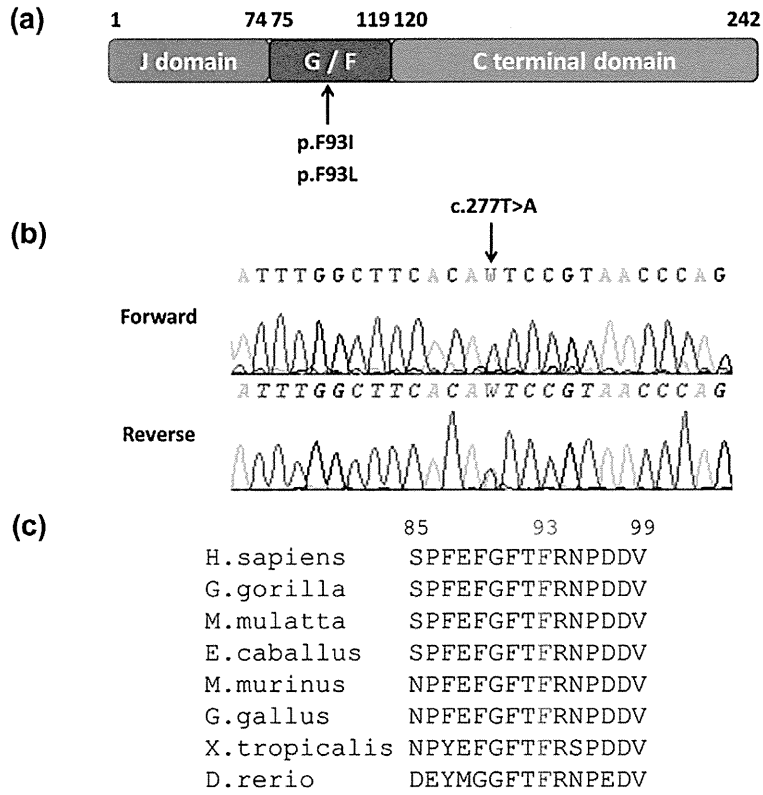

Fig. 2. Results of the mutation analysis of *DNAJB6*. (a): The domain structure of human DNAJB6 protein and the positions of the amino acid changes identified in our series and previous reports. (b): A novel heterozygous c.277T>A substitution (p.F93I) was detected in FA-1 and FA-2. (c): The phenylalanine residue at position 93 (red) is well conserved among species.

families. A c.277T>A (p.Phe93Ile) substitution in *DNAJB6* was found in Family A (FA-1 and FA-2) and a c.279C>G substitution was found in families B (FB-1), C (FC-1) and D (FD-1, FD-2, FD-3), which generated the same amino acid change of p.Phe93Leu, as previously reported [2,3] (Figs. 1 and 2). The novel substitution was not present in

the SNP database (dbSNP Build 136: http://www.ncbi.nlm.nih.gov/projects/SNP/) or 1000 Genomes (http://browser.1000genomes.org/) nor found in 100 normal Japanese individuals.

3.2. Clinical features

The clinical characteristics of the patients are summarised in Table 1.

FA-1 and FA-2 were brothers who had a novel heterozygous p.Phe93Ile amino acid substitution. Their father and younger brother also had muscle weakness that suggested autosomal dominant inheritance, although detailed medical records were not available. FA-1 and FA-2 showed slowly progressive lower limb muscle weakness or gait abnormality since their 30s. No or minimal muscle weakness was observed in the upper limbs. FA-1 also had a complete right bundle-branch block in his electrocardiogram. The serum creatine kinase (CK) levels were elevated mildly to moderately and the electromyogram (EMG) detected myogenic patterns in both patients. In the muscle magnetic resonance images (MRI) of FA-2, large areas of the thigh and posterior calf muscles were mainly affected compared with the well-preserved rectus femoris (RF), sartorius (SA), biceps (short head), gracilis and anterior lower leg muscles (Fig. 3). In agreement with the clinical findings, the upper limb muscles were well preserved in the MRI.

Four males and one female from three unrelated families carried the same c.279C>G mutation as heterozygotes. All four patients presented with a slow progressive, proximal dominant lower limb muscle weakness from middle age. Only FB-1 had been a slow runner from childhood, which may suggest childhood onset. In laboratory analysis, the serum CK levels were within threefold of the normal range while the EMG showed myogenic patterns. Computed tomography analyses (CTs) of the muscles of FD-2 (73 years old) and FB-1 showed quite similar patterns with effects in the thigh muscles, excluding the RF, SA and the posterior lower leg muscles. The paraspinal muscles were affected at the lumbar levels, especially in the outer region, whereas they were preserved in the internal area (Fig. 4). There were no signs that suggested CNS or cardiac involvement.

3.3. Muscle pathology

We analysed muscle samples from FA-1 (from quadriceps femoris), FA-2 (gastrocnemius), FB-1 (quadriceps femoris), FC-1 (biceps brachii), and FD-1 (quadriceps femoris). All five muscle specimens showed similar pathological changes including scattered atrophic fibres, some regenerating fibres, a few fibres with rimmed vacuoles (RVs) or cytoplasmic inclusions (CIs) and many with disorganised myofibrils (Fig. 5a–c). Fibre type grouping or grouped atrophy was not observed. Interestingly, a few red-green coloured nuclear inclusions were detected by mGt staining (Fig. 5d). The semi-thin sections from FD-1 also revealed some abnormal nuclei containing amorphous materials with nearly absent heterochromatin (data not shown).

Immunohistochemical analysis revealed co-accumulation of DNAJB6 with BAG3, HSPB8, HSPA8 and STUB1 in cytoplasmic inclusions of various sizes (Fig. 6). Desmin and myotilin were also stained as previously reported (data not shown) [3]. In the control muscles, DNAJB6 staining was perinuclear and it co-localised with lamin A/C (data not shown). Interestingly, in the muscles from DNAJB6 myopathy subjects, DNAJB6 was accumulated at high levels in the nucleoplasm of a few fibres and it was partially co-stained with HSPB8. However, other proteins associated with

Table 1
Clinical summary of the patients.

Patient	*DNAJB6* mutation	Age at muscle biopsy [years]	Sex	Age at onset [years]	Clinical diagnosis	Clinical course	CK [IU/L]	EMG
FA-1	c.277T>A (p.Phe93Ile)	47	M	30s	LGMD	Gait abnormality was pointed out → difficulty in climbing up stairs and easy to fall at 40s, CRBBB	268	Myogenic
FA-2		36	M	30s	LGMD	Difficulty in climbing stairs, mildly progressive lower limb weakness, atrophy in gastrocnemius muscles	1044	Myogenic
FB-1	c.279C>G (p.Phe93Leu)	44	M	25	LGMD	Slow runner in childhood, difficulty in climbing stairs at 25 years → difficulty in standing without support at 40s	696	No details
FC-1	c.279C>G (p.Phe93Leu)	64	M	50s	LGMD	Waddling gait, difficulty in standing from squatting position → difficulty in climbing stairs	523	Non specific
FD-1	c.279C > G (p.Phe93Leu)	75	M	57	LGMD	Difficulty in standing up, mildly progressive lower limb weakness → needs a wheelchair at 75 years	93	Myogenic
FD-2		68	M	55	LGMD	Progressive lower limb weakness → difficulty in walking recently, RV was seen on pathology at 60 years	165	Myogenic
FD-3		60	F	37	LGMD	Progressive lower limb weakness → difficulty in walking around 60 years	251	Myogenic

DNAJB6, DnaJ homolog, subfamily B, member 6 mutation; CK, creatine kinase; M, male; F, female; LGMD, limb-girdle.
CRBBB, complete right bundle-branch block; RV, rimmed vacuoles; EMG, electromyography.

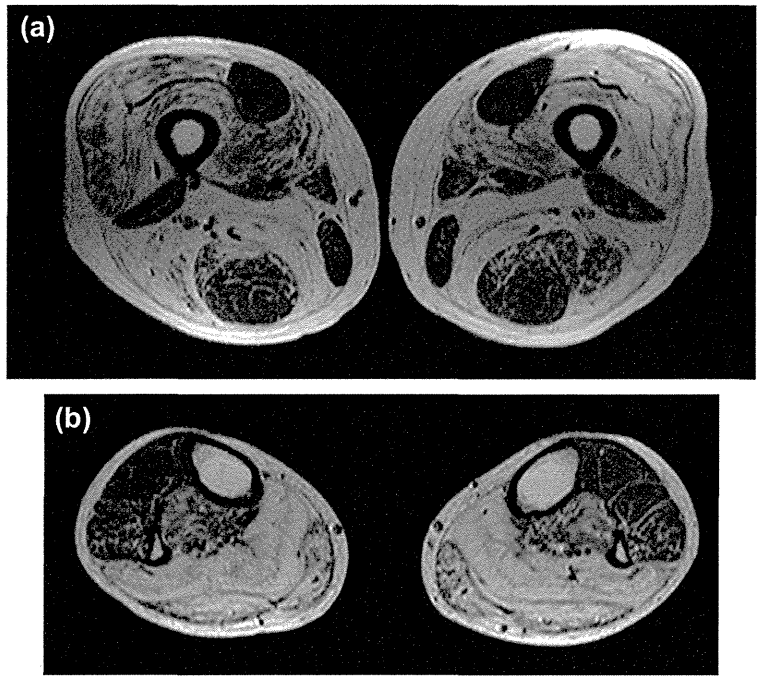

Fig. 3. Muscle images of FA-2. Images of T2-weighted thigh (a) and lower leg (b) muscles using magnetic resonance imaging. Most of the thigh and calf muscles showed fatty replacement compared with the relatively well-preserved rectus femoris, sartorius, gracilis and anterior lower leg muscles.

DNAJB6 were not observed in the nuclei. Ubiquitin, p62 and LC3 were also not stained in the nuclei. The nuclear staining and the ectopic cytoplasmic accumulations of TDP-43 were observed as previously reported (data not shown).

Semi-thin sections prepared from frozen sections revealed scattered abnormal enlarged nuclei (data not shown), although nuclear inclusions were not observed by electron microscopy using sections of frozen samples.

4. Discussion

In this study, we report seven LGMD patients from four unrelated Japanese families, who carried *DNAJB6* mutations. A novel c.277T>A substitution was considered to be the cause of an amino acid change of p.Phe93Ile in the G/F domain and was an indicator of pathogenicity. A previous report also showed that the Phe93 amino acid position was important for pathogenesis because zebrafish embryos injected with p.Phe93Ala or p.Phe93Glu mRNA showed muscle fibre detachment that resembled the p.Phe93Leu-induced phenotype [3]. The predicted p.Phe93Ile substitution affected the protein function with a SIFT (Sorting Intolerant From Tolerant) score of 0 (<0.05 indicates 'deleterious') according to the SIFT database (http://sift.jcvi.org/), whereas the PolyPhen 2 program (http://genetics.bwh.harvard.edu/pph2/) indicated that it was probably damaging with a score of 0.999. The dbSNP Build 136 and 1000 Genome databases did not list this variant. On the basis of these data, we confirmed that the c.277T>A substitution was a novel disease-associated mutation. The nucleotide substitution of c.279C>G (p.Phe93Leu) was previously reported and was common in families B, C and D [3]. All reported mutations linked with *DNAJB6*, including the results of this study, are located in the G/F domain. The role of the G/F domain is still not understood in mammalian cells, although the G/F domain is associated with substrate recognition and the formation of a stable substrate complex in the bacterial ortholog [6]. The G/F domain may have an important role in preserving muscle functions in humans.

All patients in our series, with the exception of FB-1, presented with slowly progressive muscle weakness, mainly in the lower limbs, from middle age. In contrast, FB-1 indicated childhood onset. The youngest previously reported age of onset among patients with the *DNAJB6* mutation was 14 years [3], hence, the DNAJB6 myopathy may have a childhood onset. The muscle images of DNAJB6 myopathy in our series all shared the same characteristics as previously reported [1]. The rectus femoris, sartorius and anterior calf muscles were relatively preserved, whereas the other leg muscles were severely affected. The upper limb muscles were also well preserved. In addition, paraspinal muscle involvement was prominent at the lumbar level. The expression of DNAJB6 is ubiquitous [7] but skeletal muscles

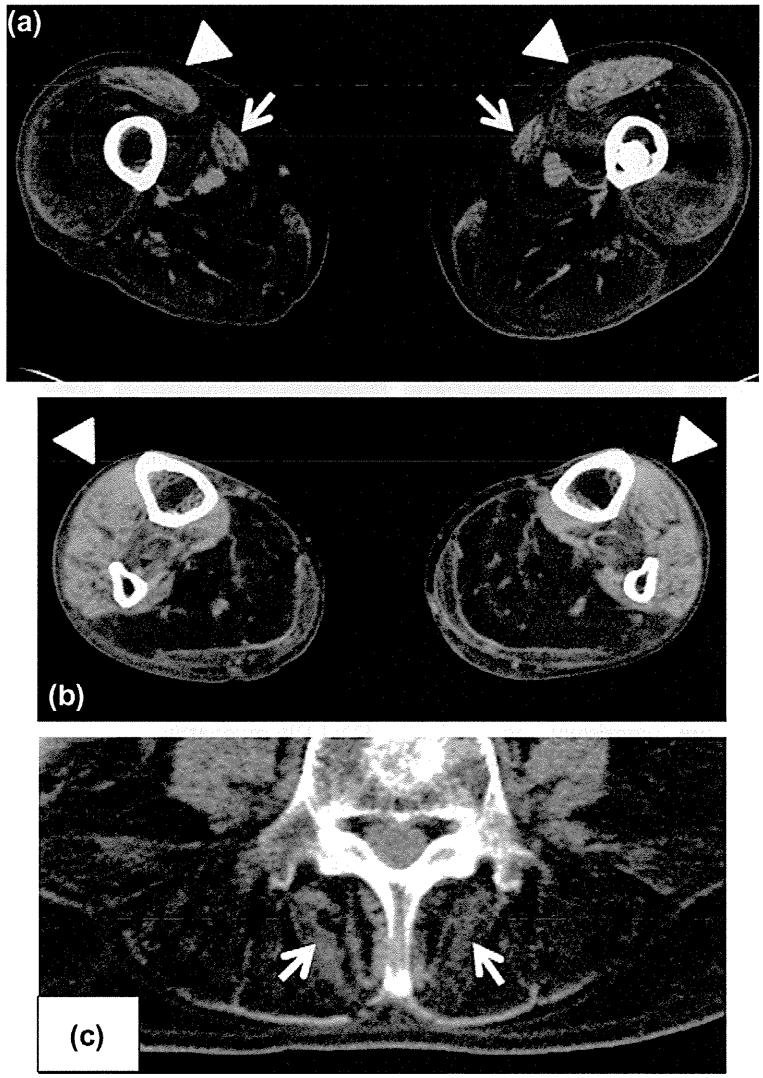

Fig. 4. Muscle images of FD-2. Computed tomography analyses of the thigh (a), lower leg muscles (b) and paraspinal muscles at the lumbar level (c). The rectus femoris (arrowheads) and sartorius muscles (arrows) are relatively well preserved (a). Anterior calf muscles are relatively preserved (arrow heads), compared to posterior side (b). The paraspinal muscles are affected, especially in the outer region, whereas their inner regions are well preserved (c, arrows).

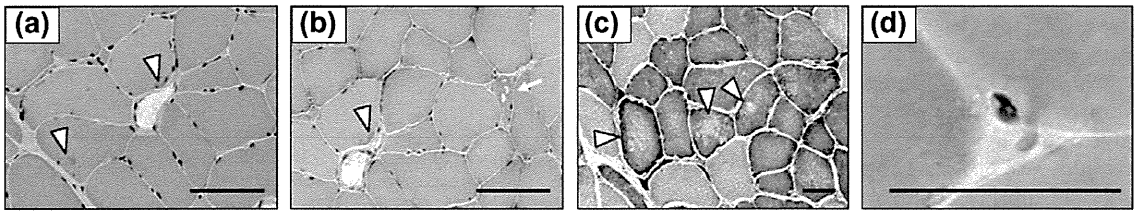

Fig. 5. Histological analyses of muscle of FD-1. Hematoxylin and eosin (a) and modified Gomori trichrome (b) staining showed a few tiny cytoplasmic inclusions (white arrowheads) and rimmed vacuoles (white arrow). NADH-tetrazolium reductase staining revealed disorganised myofibrils with a moth-eaten appearance (c). Modified Gomori trichrome staining indicates an abnormal nucleus with inclusion (d). Bar = 50 μm.

are preferentially involved. However, the cause of the selective muscle involvement remains unclear.

The muscle pathology of DNAJB6 myopathy is characterised by the presence of rimmed vacuoles,

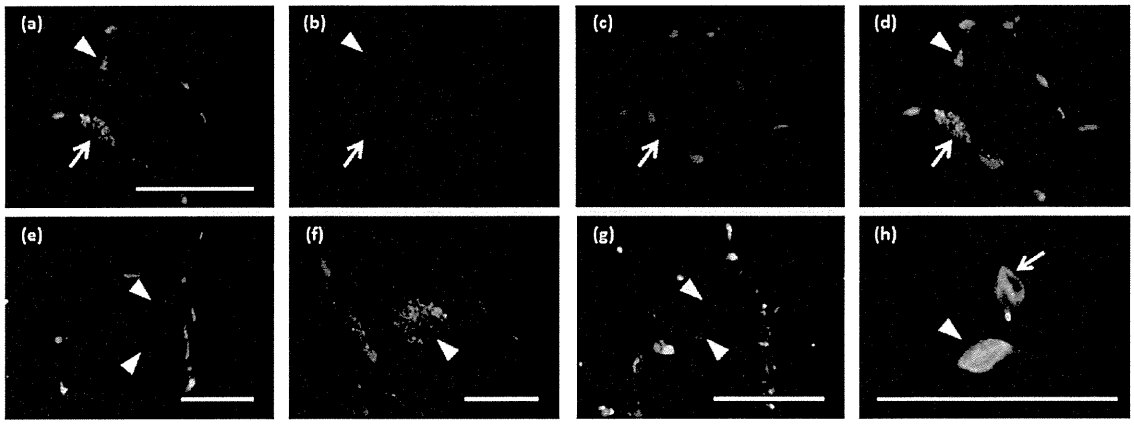

Fig. 6. Immunohistochemistry of FA-2, FC-1 and FD-1 (a: DNAJB6; b: HSPB8; c: DAPI; d: merge). In the muscle from FC-1, intranuclear accumulation of DNAJB6, partially co-stained with HSPB8 was observed (arrow). Cytoplasmic inclusions were also co-stained as DNAJB6 and HSPB8 (arrowhead). (e–g: Merged staining of DNAJB6 (green), DAPI (blue) and BAG3 (e, red) or HSPA8 (f, red) or STUB1 (g, red)). Cytoplasmic inclusions of DNAJB6 co-stained with BAG3, HSPA8 or STUB1 were observed (arrowhead). (h) Merged staining of DNAJB6 and lamin A/C. DNAJB6 merged with lamin A/C (arrow). Intranuclear accumulations of DNAJB6 were observed in a few nuclei (arrowhead). Bar = 50 μm.

cytoplasmic inclusions and disorganised myofibrils [1–3]. All affected individuals in our cohort shared these pathological features. These changes are consistent with the characteristics of myofibrillar myopathy (MFM). MFM is a group of clinically or genetically heterogeneous but pathologically similar muscle disorders that are defined by the presence of disorganised myofibrils and cytoplasmic desmin-positive inclusions [8,9]. Fibres with rimmed vacuoles are often observed. Given these pathological muscle changes, DNAJB6 myopathy can also be characterised as MFM. All six known causative genes of MFM encode Z-disc associated proteins [10–15]. Of these, *BAG3* and *CRYAB* encode co-chaperones and are involved with protein quality control [16,17]. Immunohistochemical analysis revealed that DNAJB6 accumulated in the cytoplasm where it was co-stained along with HSPB8, BAG3, HSPA8 and STUB1, which are members of the chaperone-assisted selective autophagy (CASA) complex [18]. DNAJB6 can interact with the CASA protein complex and is associated with protein quality control [18]. The co-accumulation of DNAJB6 with CASA proteins and the presence of rimmed vacuoles in the cytoplasm may suggest an altered protein degradation system in the skeletal muscles with DNAJB6 myopathy.

In this study, we observed co-staining of DNAJB6 with lamin A/C in normal control muscles, indicating the presence of DNAJB6 in the perinuclear region. In addition, we detected the intranuclear accumulation of DNAJB6 with HSPB8. Semi-thin sections revealed scattered abnormal enlarged nuclei. Detailed ultrastructural analysis of nuclei was difficult using sections of frozen samples. Thus, further analyses are required to elucidate the roles of DNAJB6 in the nucleus, to clarify the specific role of DNAJB6 in human muscles and to understand the pathological mechanism of DNAJB6 myopathy.

Acknowledgement

This study was supported by a Grant-in-Aid for Scientific Research from the Japan Society for the Promotion of Science, Research on Psychiatric and Neurological Diseases and Mental Health, Research on Measures for Intractable Diseases, Health Labour Sciences Research Grant for Nervous and Mental Disorders (20B-12, 20B-13) from the Ministry of Health, Labour and Welfare, and an Intramural Research Grant (23-4, 23-5, 23-6) for Neurological and Psychiatric Disorders of NCNP. The authors thank Ms. K. Goto, Ms. M. Takami, Dr. S. Suzuki and Mr. K. Ogata (NCNP) for the technical assistance. The authors would like to thank Enago (www.enago.jp) for the English language review.

References

[1] Sandell S, Huovinen S, Sarparanta J, et al. The enigma of 7q36 linked autosomal dominant limb girdle muscular dystrophy. J Neurol Neurosurg Psychiatry 2010;81:834–9.
[2] Harms MB, Sommerville RB, Allred P, et al. Exome sequencing reveals DNAJB6 mutations in dominantly-inherited myopathy. Ann Neurol 2012;71:407–16.
[3] Sarparanta J, Jonson PH, Golzio C, et al. Mutations affecting the cytoplasmic function of the co-chaperone DNAJB6 cause limb-girdle muscular dystrophy. Nat Genet 2012;44:450–5.
[4] Hageman J, Rujano MA, van Waarde MA, et al. A DNAJB chaperone subfamily with HDAC-dependent activities suppresses toxic protein aggregation. Mol Cell 2010;37:355–69.

[5] Dai YS, Xu J, Molkentin JD. The DnaJ-related factor Mrj interacts with nuclear factor of activated T cell c3 and mediates transcriptional repression through class II histone deacetylase recruitment. Mol Cell Biol 2005;25:9936–48.
[6] Perales-Calvo J, Muga A, Moro F. Role of DnaJ G/F-rich domain in conformational recognition and binding of protein substrates. J Biol Chem 2010;285:34231–9.
[7] Hageman J, Kampinga HH. Computational analysis of the human HSPH/HSPA/DNAJ family and cloning of a human HSPH/HSPA/DNAJ expression library. Cell Stress Chaperones 2009;14:1–21.
[8] Nakano S, Engel AG, Waclawik AJ, Emslie-Smith AM, Busis NA. Myofibrillar myopathy with abnormal foci of desmin positivity. I. Light and electron microscopy analysis of 10 cases. J Neuropathol Exp Neurol 1996;55:549–62.
[9] De Bleecker JL, Engel AG, Ertl BB. Myofibrillar myopathy with abnormal foci of desmin positivity. II. Immunocytochemical analysis reveals accumulation of multiple other proteins. J Neuropathol Exp Neurol 1996;55:563–77.
[10] Goldfarb LG, Park KY, Cervenáková L, et al. Missense mutations in desmin associated with familial cardiac and skeletal myopathy. Nat Genet 1998;19:402–3.
[11] Vicart P, Caron A, Guicheney P, et al. A missense mutation in the alphaB-crystallin chaperone gene causes a desmin-related myopathy. Nat Genet 1998;20:92–5.
[12] Selcen D, Engel AG. Mutations in myotilin cause myofibrillar myopathy. Neurology 2004;62:1363–71.
[13] Selcen D, Engel AG. Mutations in ZASP define a novel form of muscular dystrophy in humans. Ann Neurol 2005;57:269–76.
[14] Vorgerd M, van der Ven PF, Bruchertseifer V, et al. A mutation in the dimerization domain of filamin c causes a novel type of autosomal dominant myofibrillar myopathy. Am J Hum Genet 2005;77:297–304.
[15] Selcen D, Muntoni F, Burton BK, et al. Mutation in BAG3 causes severe dominant childhood muscular dystrophy. Ann Neurol 2009;65: 83–9.
[16] Hishiya A, Salman MN, Carra S, Kampinga HH, Takayama S. BAG3 directly interacts with mutated alphaB-crystallin to suppress its aggregation and toxicity. PLoS One 2011;6:e16828.
[17] Arai H, Atomi Y. Chaperone activity of alpha B-crystallin suppresses tubulin aggregation through complex formation. Cell Struct Funct 1997;22:539–44.
[18] Arndt V, Dick N, Tawo R, et al. Chaperone-assisted selective autophagy is essential for muscle maintenance. Curr Biol 2010; 20:143–8.

SCIENTIFIC REPORTS

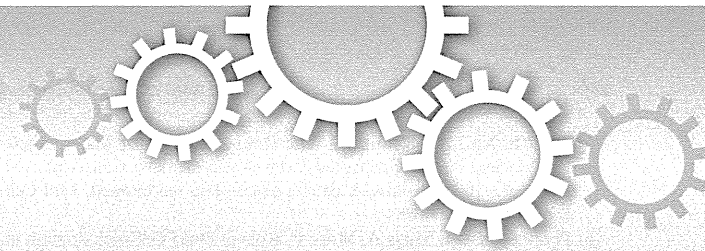

OPEN

SUBJECT AREAS:
MECHANISMS OF DISEASE
ANTISENSE OLIGO
DRUG DELIVERY
RNA SPLICING

Received
18 March 2013

Accepted
21 June 2013

Published
22 July 2013

Correspondence and requests for materials should be addressed to S.I. (cishiura@mail.ecc.u-tokyo.ac.jp)

Ultrasound-enhanced delivery of Morpholino with Bubble liposomes ameliorates the myotonia of myotonic dystrophy model mice

Michinori Koebis[1], Tamami Kiyatake[1], Hiroshi Yamaura[1], Kanako Nagano[1], Mana Higashihara[2], Masahiro Sonoo[3], Yukiko Hayashi[4], Yoichi Negishi[5], Yoko Endo-Takahashi[5], Dai Yanagihara[1], Ryoichi Matsuda[1], Masanori P. Takahashi[6], Ichizo Nishino[4] & Shoichi Ishiura[1]

[1]Graduate School of Arts and Sciences, the University of Tokyo, Tokyo, Japan, [2]Division of Neurology, Department of Internal Medicine 3, National Defense Medical College, Saitama, Japan, [3]Department of Neurology, Teikyo University School of Medicine, Tokyo, Japan, [4]Department of Neuromuscular Research, National Institute of Neuroscience, National Center of Neurology and Psychiatry (NCNP), Tokyo, Japan, [5]Department of Drug Delivery and Molecular Biopharmaceutics, School of Pharmacy, Tokyo University of Pharmacy and Life Sciences, Tokyo, Japan, [6]Department of Neurology, Osaka University Graduate School of Medicine, Osaka, Japan.

Phosphorodiamidate morpholino oligonucleotide (PMO)-mediated control of the alternative splicing of the chloride channel 1 (*CLCN1*) gene is a promising treatment for myotonic dystrophy type 1 (DM1) because the abnormal splicing of this gene causes myotonia in patients with DM1. In this study, we optimised a PMO sequence to correct *Clcn1* alternative splicing and successfully remedied the myotonic phenotype of a DM1 mouse model, the HSA^{LR} mouse. To enhance the efficiency of delivery of PMO into HSA^{LR} mouse muscles, Bubble liposomes, which have been used as a gene delivery tool, were applied with ultrasound exposure. Effective delivery of PMO led to increased expression of Clcn1 protein in skeletal muscle and the amelioration of myotonia. Thus, PMO-mediated control of the alternative splicing of the *Clcn1* gene must be important target of antisense therapy of DM1.

Myotonic dystrophy type 1 (DM1) is caused by expansion of the CTG repeat in the 3′ untranslated region (UTR) of the *DMPK* gene[1–4]. Patients with DM1 show multi-systemic symptoms, including muscle wasting, muscle weakness, myotonia, cardiac conduction defect, cataracts, mental retardation and insulin resistance[5]. A patient, however, does not always present with all of these symptoms and the severity of the disease varies among individuals. Among the symptoms, myotonia is the most prominent and common phenotype of DM1: most patients feel muscle stiffness and difficulty in relaxing muscles soon after developing the disease.

The characteristic feature of the pathology of DM1 is the aberrant regulation of dozens of alternative splicing events, and some of the abnormal splicing events have been suggested to be involved in some of the symptoms[6–10]. Myotonic discharge is thought to be caused by the aberrant alternative splicing of the chloride channel 1 (*CLCN1*) gene[11,12]. In patients with DM1, extra exons from intron 6 are spliced into the *CLCN1* mRNA, leading to the appearance of a premature termination codon in the subsequent exon, degradation of the mRNA by nonsense-mediated decay and decreased expression of CLCN1 protein[11]. The idea that abnormal splicing of the *CLCN1* gene causes myotonia is strongly supported by the fact that the *CLCN1* gene is the only gene responsible for congenital myotonia, and the identification of multiple mutations in patients with the disease and their families[13]. Wheeler and his colleagues corrected the abnormal splicing of the *Clcn1* gene in a DM1 mouse model, the HSA^{LR} mouse, by using an antisense oligonucleotide (AON) and successfully alleviated the myotonic phenotype[14]. Thus, correction of the abnormally regulated splicing is a promising treatment for DM1.

An AON is a short, synthetic nucleic acid molecule with a sequence complementary to a target transcript. It can be used to manipulate an alternative splicing event: the AON that binds to the region around the target exon, specifically splice sites or splicing enhancer domains, physically blocks assembly of the spliceosome on the exon and induces exon skipping[15]. The efficacy of an AON is dependent on its half-life, affinity for its target RNA and *in*

vivo kinetics. A variety of AON molecules with 2′-*O* modifications and/or unnatural backbones have been developed to improve nuclease resistance and affinity for RNA[15]. Among them, Morpholino (also referred as phosphorodiamidate morpholino oligonucleotide [PMO]) is one of the most hopeful AONs. PMO has morpholine rings linked with phosphorodiamidate linkages in its backbone instead of deoxyribose and phosphodiester bonds. Due to its completely unnatural chemistry, PMO is hardly recognised by cellular nucleases. It has higher affinity for RNA than for DNA; the T_m value of a hybrid of PMO and RNA is much higher than that of DNA and RNA[16]. Several papers have reported the local and systemic administration of PMO to mice and dogs. For example, when a high dose of PMO (3 g/kg) was administrated intravenously into the *mdx* mouse, a mouse model of Duchenne muscular dystrophy, the PMO entered skeletal muscle without any assistive delivery reagent[17]. However, unlike mdx mice, muscle penetration of Evans Blue dye did not increase in HSA^{LR} and wild-type mice[18], which indicated a physical barrier to PMO uptake should be grater in HSA^{LR} than in *mdx*. In preceding reports on PMO treatment in HSA^{LR}, intravenous administration of CAG25 PMO led no detectable improvements in *Serca1* splicing in HSA^{LR} mice[19], and even when PMO was injected intramuscularly its uptake was limited to the needle track[14]. In these studies, they used electroporation to administer unmodified PMO intramuscularly, so we investigated a less invasive PMO delivery method to develop PMO treatment for DM1.

Recently, ultrasound exposure has been used for the intracellular delivery of molecules such as dextran, plasmid DNA and siRNA. If ultrasound is sufficiently strong, it will generate microscopic vacuum bubbles in a solution by a process known as inertial cavitation. The bubbles immediately collapse, producing a shock wave, which is believed to transiently increase the permeability of cell membranes in the vicinity. Inertial cavitation is enhanced by using micro bubbles of echo-contrast gas. This method has been applied to gene delivery into various mouse tissues, including skeletal muscle, liver and tumour tissues[20–22]; however, introducing genes into deep tissues with microbubbles is difficult because of their size and instability. To overcome these problems, we previously developed a novel drug delivery reagent coined "Bubble liposomes", polyethylene glycol-modified liposomes (PEG liposomes) encapsulating echo-contrast gas[23]. Owing to the stability in serum and uniform microscopic size of PEG liposomes, we successfully delivered genes and siRNA into several tissues[24–28]. However, does the Bubble liposome-ultrasound delivery system efficiently deliver PMO into skeletal muscles in the HSA^{LR} mice? In this study, we examined the ability of the Bubble liposome-ultrasound system to deliver PMO into skeletal muscles of HSA^{LR} mice as a treatment for abnormal splicing.

We newly designed antisense PMOs targeting exon 7A of the *Clcn1* gene and delivered them into HSA^{LR} mice. The PMOs were successfully delivered into skeletal muscles by the Bubble liposome-ultrasound system, which decreased the inclusion of exon 7A *in vivo*. Furthermore, the injection of PMO ameliorated the myotonic phenotype of the model mice. Our results suggest that Bubble liposomes should be effective for delivering PMOs into muscle tissues and can be applied to PMO treatment of DM1.

Results

We first determined the optimal target sequence of the *Clcn1* pre-mRNA to promote skipping of exon 7A. To achieve this, we used a *Clcn1* minigene and examined its alternative splicing using a cell culture-based assay. The minigene contains the genomic region from exon 6 to exon 7 of the murine *Clcn1* gene. When it was transfected into COS-7 cells, approximately 50% of transcripts contained exon 7A (Fig. 1b, minigene only). To screen for an optimal AON sequence, we used 25-mer phosphorothioate 2′ *O*-methyl (PS2OMe) RNA, which can regulate alternative splicing by sterically preventing spliceosomal assembly, just like PMO. We examined PS2OMe RNA molecules that covered the whole of exon 7A (1–25, 26–50, 51–75 and 76–90) and the boundary of intron 6 and exon 7A (−10–15). We transfected the minigene together with the PS2OMe RNA into COS-7 cells and analysed the alternative splicing of the minigene. We found that −10–15 and 1–25 PS2OMe significantly reduced the rate of inclusion of exon 7A, with 1–25 PS2OMe being the most effective molecule (Fig. 1b).

Previously, we identified the 8 nt at the 5′ end of exon 7A as an exonic splicing enhancer (ESE) essential for basal inclusion of the exon[29]. Given that both −10–15 and 1–25 PS2OMe covered the ESE, and that 1–25 PS2OMe seemed to be more effective at excluding exon 7A, we speculated that another ESE (16–25) would be located in the region +16 to +25, and that 1–25 PS2OMe would not share it with −10–15 PS2OMe. To examine this possibility, we tested whether 16–40 PS2OMe enhanced normal splicing. 16–40 PS2OMe markedly reduced the rate of inclusion of exon 7A of the *Clcn1* minigene (Supplementary Fig. S1). As 26–50 PS2OMe did not change the alternative splicing, we conclude that the other ESE (16–25) is important for exon 7A inclusion. Thus, we used 1–25 AON, which targeted both ESEs, in subsequent experiments.

PS2OMe is highly resistant to nuclease-mediated degradation owing to its phosphorothioate linkages; however, it is still degraded slowly and releases monomers that have a toxic, free phosphorothioate group. In contrast, PMO is remarkably resistant to degradation and is not noxious. Therefore, we next investigated whether a PMO with the same sequence as 1–25 PS2OMe also improved the alternative splicing of exon 7A by using the cell culture-based splicing assay (Fig. 1c). The −11–14 PMO we used here had the same sequence as that Wheeler and his colleagues used in a previous study[14]. RT-PCR analysis showed that both 1–25 and −11–14 PMOs significantly reduced exon 7A inclusion. Although the effect of 1–25 PMO was greater than that of −11–14 PMO, no statistically significant difference was observed between them.

1–25 PMO was so effective at improving alternative splicing of the *Clcn1* minigene in cultured cells that we expected it to work well *in vivo*. To test whether 1–25 PMO could work *in vivo*, we administrated 60 μg of 1–25 PMO intramuscularly four times at weekly intervals into the *tibialis anterior* (TA) muscles of HSA^{LR} mice. The alternative splicing of the *Clcn1* gene was moderately improved, with an approximately 30% decrease in exon 7A inclusion. Electromyography (EMG) with a single needle electrode, however, revealed that the occurrence of myotonia was not altered by PMO injection (Supplementary Fig. S2). Because 60 μg of PMO was quite a high dose for administration into a single muscle, we assumed that an effective delivery system would be required to introduce 1–25 PMO into muscle tissues. We therefore examined the usefulness of ultrasound-enhanced delivery with Bubble liposomes for PMO delivery. We administrated 20 μg of 1–25 PMO three times at weekly intervals into the TA muscles of HSA^{LR} mice with or without Bubble liposomes and ultrasound (Fig. 2). RT-PCR analysis revealed that the rate of inclusion of exon 7A decreased to its lowest level when both Bubble liposomes and ultrasound were applied, indicating that use of the combination of Bubble liposomes and ultrasound could enhance PMO delivery efficiency.

We next investigated whether 1–25 PMO could cure myotonic symptoms in HSA^{LR} mice when delivered using the Bubble liposome-ultrasound system. We administrated 1–25 PMO as described above. Three weeks later, we harvested the injected muscles and conducted RT-PCR and immunohistological analyses. RT-PCR showed that 1–25 PMO decreased the inclusion of exon 7A to a level comparable to that in wild-type FVB/n mice (Fig. 3a). We checked four other alternative splicing events, *Cypher* (*Ldb3*) exon 11, *Mbnl1* exon 5, *Ryr1* exon 70 and *Serca1* exon 22, which are known to be abnormally regulated in patients with DM1and HSA^{LR} mice[30]. We found that the alternative splicing of none of them was changed by

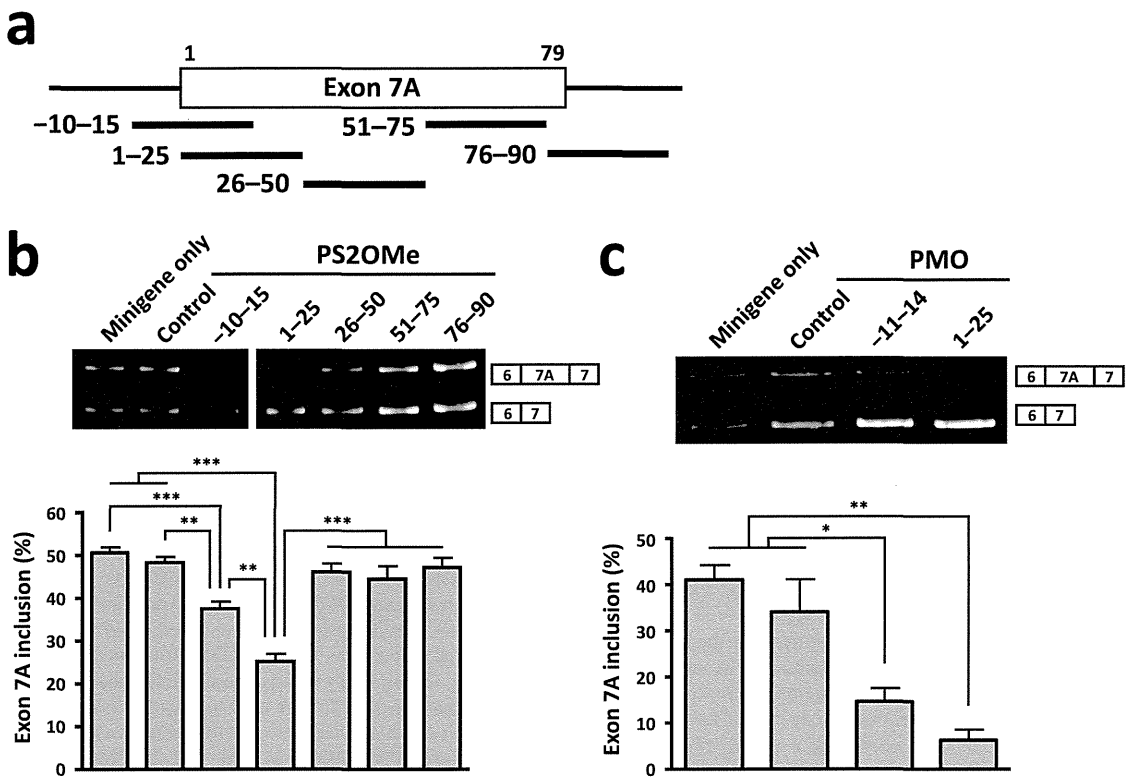

Figure 1 | AON-mediated exclusion of *Clcn1* exon 7A in COS-7 cells. (a) Locations of the target sites of AONs (thick black lines) along the *Clcn1* pre-mRNA. The numbers over exon 7A (rectangle) indicate the positions of nucleotides. (b) Cellular splicing assay to detect the exclusion of exon 7A of the *Clcn1* minigene by PS2OMe RNA in COS-7 cells. 1–25 was the most successful AON. A representative result is shown above and the bars indicate mean and s.e.m. ($n = 6$). (c) The same assay as in (b) except that PMOs were used. 1–25 PMO decreased the inclusion of exon 7A effectively ($n = 3$). Statistical significance was analysed by Tukey's multi-comparison test (* $P < 0.05$, ** $P < 0.01$, *** $P < 0.001$).

the injection of 1–25 PMO (Fig. 3b); thus, the effect of the PMO was specific to the alternative splicing of the *Clcn1* gene.

The abnormal splicing of *Clcn1* is believed to cause myotonia by introducing a premature termination codon into the subsequent exon and by decreasing the expression of the Clcn1 protein via nonsense-mediated mRNA decay. Thus, we examined whether 1–25 PMO restored the expression of Clcn1 protein in HSA^{LR} mice. Immunofluorescence analysis of TA muscles showed the sarcolemmal localisation of Clcn1 protein in wild-type muscle, but such a pattern was not detected in saline-injected HSA^{LR} mice. The injection of 1–25 PMO clearly restored the sarcolemmal distribution, demonstrating that correction of the abnormal splicing of the *Clcn1* gene led to the normal expression of its protein (Fig. 3c).

Finally, we investigated whether injection of 1–25 PMO improved the myotonic phenotype of HSA^{LR} mice. Electromyographic analyses showed bursts of action potentials after electrical stimulation (4–8 V) in HSA^{LR} mice, but not in wild-type mice (Fig. 4a). Myotonia occurred even in denervated muscles (data not shown), which indicates that it was not caused by hyperactivation of motor neurones, but by increased excitability of the sarcolemma. Myotonic EMG activities continued for 1 to 3 s and their average duration was 1.27 s in saline-treated TA muscles. The injection of 1–25 PMO decreased their duration, but the change was not statistically significant; the integrated EMG (iEMG) was reduced by the PMO administration ($P < 0.05$). The decreased iEMG indicated that 1–25 PMO mitigated the hyperexcitability of the HSA^{LR} muscles.

These results suggest that 1–25 PMO could improve the function of the *Clcn1* gene in the DM1 model mouse at the RNA, protein and

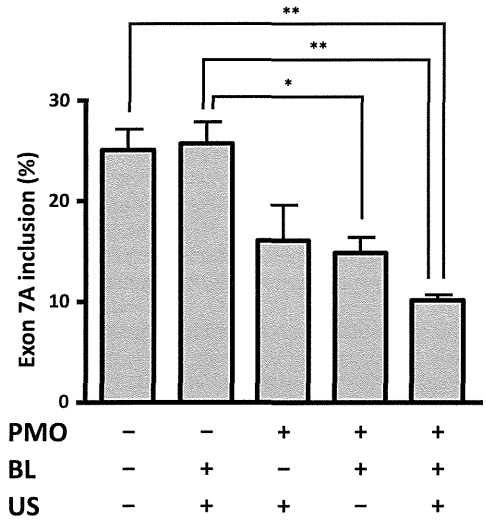

Figure 2 | PMO delivery by the combination of Bubble liposomes and ultrasound. 1–25 PMO (20 μg) or saline was locally administrated into TA muscles of HSA^{LR} mice with/without Bubble liposomes (BLs) and ultrasound (US). The inclusion rate of exon 7A decreased most when both Bubble liposomes and ultrasound were applied. ($n = 3$). The bars indicate mean and s.e.m., and statistical significance was analysed by Tukey's multi-comparison test (* $P < 0.05$, ** $P < 0.01$).

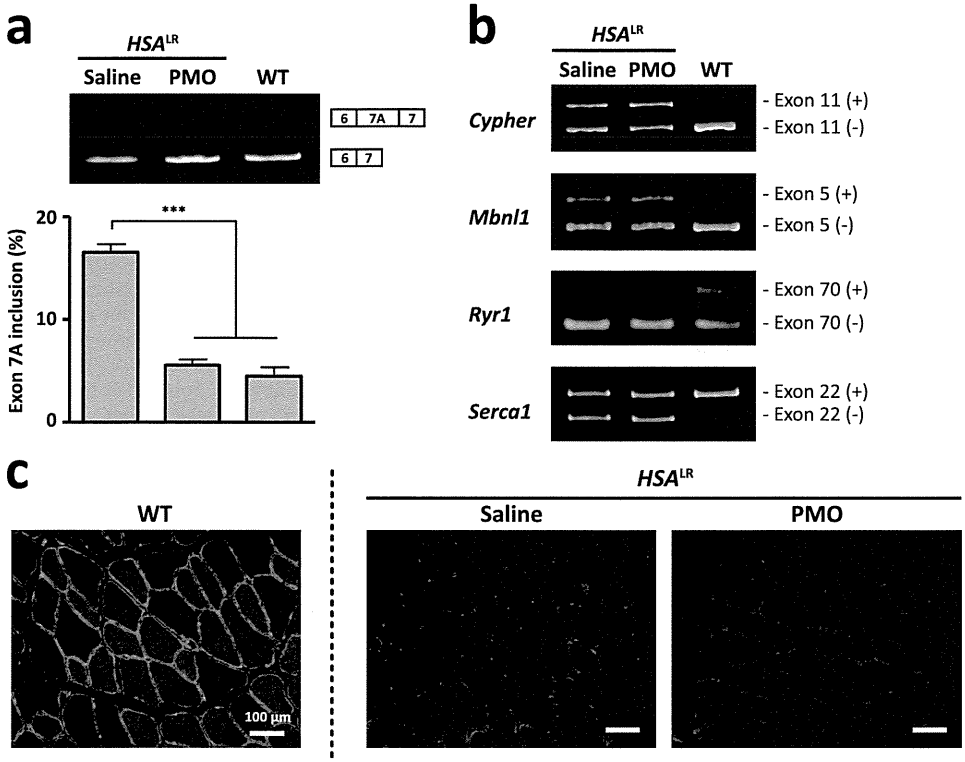

Figure 3 | *In vivo* improvement of aberrant splicing of the *Clcn1* gene by 1–25 PMO. (a) The alternative splicing of *Clcn1* exon 7A in HSA^{LR} and WT mice. 1–25 PMO (20 μg) or saline was locally administrated into TA muscles of HSA^{LR} mice. The ratio of the splicing variant containing exon 7A in thevPMO-injected muscles decreased to a level comparable with that in WT muscle ($n = 5$). The bars indicate mean and s.e.m., and statistical significance was analysed by Tukey's multi-comparison test (*** $P < 0.001$). (b) Abnormal splicing of other genes in HSA^{LR} mice was not affected by 1–25 PMO. (c) Immunofluorescence analysis of transverse sections of TA muscle with an anti-Clcn1 antibody. Injection of 1–25 PMO restored the sarcolemmal localisation of Clcn1 protein in TA muscles of HSA^{LR} mice.

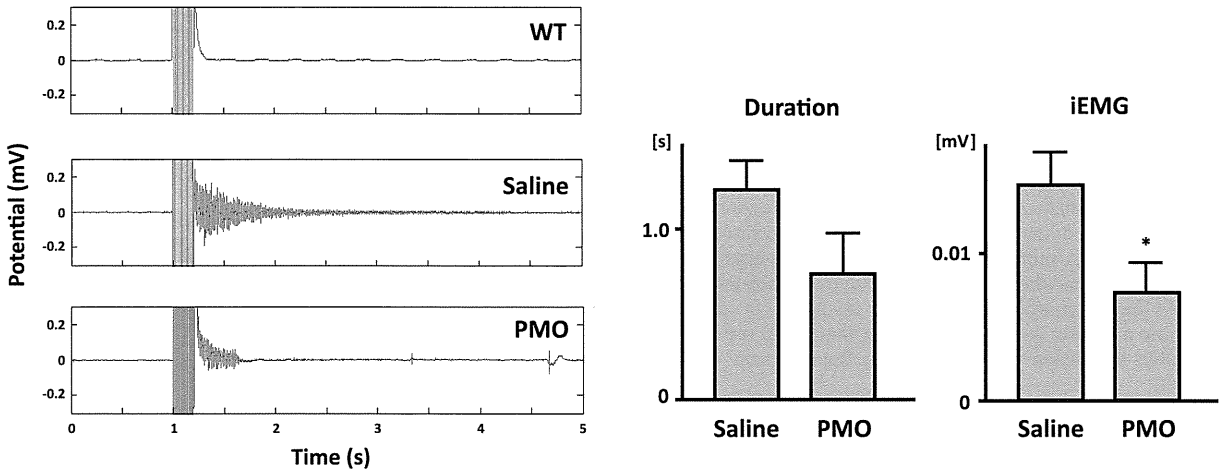

Figure 4 | Reduction of myotonic discharge by 1–25 PMO in HSA^{LR} mice. (a) Representative EMG signals of TA muscle. Tibialis muscle was electrically stimulated 1 s after the EMG recording started. In the HSA^{LR} muscle, repetitive discharges that were absent in the WT muscle could be seen. (b)vDuration of myotonic discharge and integrated EMG (iEMG). 1–25 PMO significantly reduced iEMG in HSA^{LR} muscle (saline, $n = 6$; 1–25 PMO, $n = 7$).The bars indicate mean and s.d., and statistical significance was analysed by Student's *t*-test (* $P < 0.05$).

phenotypic levels, and that the Bubble liposome-ultrasound system should be capable of delivering enough PMO to ameliorate myotonia.

Discussion

The greatest advantage of PMO is its remarkable innocuity. According to a report from Gene Tools, administration of a single 700 mg/kg dose of PMO to a mouse did not cause any obvious acute toxicity[31], while the 50% lethal dose of phosphorothioate DNA, a first-generation antisense oligonucleotide, was estimated to be 750 mg/kg in mice[32]. The high pharmaceutical potential of PMO is also supported by the fact that safety issues were not raised following its administration to mice and humans; however, PMO must overcome the low permeability of the cell membranes to achieve a significant effect on alternative splicing. Because of the inefficient cellular uptake of PMO, systemic delivery and functional splicing modification were not successful in a mouse model[33]. Therefore, for the clinical application of PMO, establishing an effective delivery method is essential.

The major achievement in this study was that we increased the efficiency of PMO delivery using Bubble liposomes and ultrasound. The use of the ultrasound-mediated delivery system with Bubble liposomes improved the alternative splicing of the *Clcn1* gene in HSA^{LR} mice to a level comparable to that of wild-type mice and decreased myotonic discharges, indicating that the delivery system increased introduction of 1–25 PMO into skeletal muscle. Our results show that the intramuscular injection itself delivered the PMO into muscle to some extent, and so the intramuscular injection might have contributed to the relief of the pathology. However, the Bubble liposome- and ultrasound-mediated enhancement of delivery efficiency suggests that the new delivery system will have a beneficial effect over much less invasive injection, such as intravenous injection, which cannot by itself be expected to promote the entry of PMO into skeletal muscle[19].

A fair amount of the *Clcn1* splicing variant without exon 7A was expressed even in the HSA^{LR} mouse. Because the myotonic discharge of a HSA^{LR} mouse was remedied by correcting *Clcn1* alternative splicing in a previous study[14], abnormal splicing of the gene must be the primary cause of myotonia. The expression levels of the "normal" splicing variant in saline-injected muscles were 57% of that in the wild-type muscles. PMO injection increased the expression about 1.4-fold to 78% of that in wild-type mice. As *Clcn1* heterozygous mutant mice did not show a myotonic phenotype[34], the myotonia in HSA^{LR} mice was unlikely to have been caused by haploinsufficiency of full-length Clcn1 protein. Instead, the truncated protein translated from the exon 7A-countaining mRNA may have dominant-negative activity, since full-length Clcn1 protein functions in a dimeric form. Berg *et al.* showed that the truncated Clcn1 protein did not function as a chloride channel, but rather disturbed the channel activity of full-length Clcn1 protein[35]. In this study, expression of the splicing variant containing exon 7A was decreased by 40% in the PMO-administered group. Thus, this may have contributed to the improvement of the pathology, as well as the increased expression of the exon 7A skipping variant. The dominant-negative hypothesis suggests that the AON therapy should completely prevent exon 7A inclusion when used to treat myotonia, in contrast to Duchenne muscular dystrophy, in which the partial restoration of dystrophin expression could lead to the improvement of muscle strength.

In the course of our search for the optimal PMO sequence to correct *Clcn1* splicing, we found that 1–25 and 16–40 PMOs suppressed the inclusion of exon 7A well, but that 26–50 PMO did not. The fact that steric blocking of the 16–25 region promoted exon skipping indicates that proteins that bind to this region are essential for exon 7A recognition. Previously, we showed that the 8 nt at the 5′ end of exon 7A serve as an ESE and that an RNA-binding protein, Mbnl1, prevented the inclusion of exon 7A by binding to the ESE[29]. Unlike the ESE, the sequence of the 16–25 region was pyrimidine-rich and did not contain the Mbnl1-recognition motif, YGCY. It remains to be determined which proteins bind to the region to regulate exon 7A splicing.

In this study, we tried to cure DM1 model mice using a PMO targeted to *Clcn1*. However, considering that dozens of genes are abnormally spliced in patients with DM1, it might be impractical to treat all symptoms due to mis-splicing of such genes with AONs at the same time. DM1 is caused by expansion of the CTG repeats in the 3′ UTR region of the DMPK gene. Transcripts with these expanded repeats sequester Mbnl proteins, which regulate alternative splicing, leading to global alternative splicing dysfunction[36]. Thus, expanded CUG repeat-containing RNA must be the most important target of antisense therapy for DM1, and many groups have studied the use of CAG repeat-containing AONs to dissociate Mbnl1 proteins from CUG repeat-containing RNA. Some trials to treat DM1 model mice with CAG AONs were successful[19,37], but here again the obstacle to clinical application of the AONs was the lack of an efficient delivery method. Our ultrasound-mediated delivery system with Bubble liposomes must have a beneficial effect on the delivery of CAG-containing AONs.

Methods

AONs. Phosphorothioate 2′ *O*-methyl RNA oligonucleotides and phosphorodiamidate morpholino oligonucleotides were purchased from IDT (Coralville, IA, USA) and Gene Tools (Philomath, OR, USA), respectively. The sequences of the oligonucleotides are listed in Supplementary Table ST1. Both AONs were dissolved in water.

Construct. The *Clcn1* minigene has been described previously[29]. Briefly, a *Clcn1* minigene fragment covering exons 6 to 7 was amplified from mouse genomic DNA by PCR and inserted into the *BglII-SalI* sites of pEGFP-C1 (Clontech Laboratories, Mountain View, CA, USA).

Cellular splicing assay. COS-7 cells were cultured in Dulbecco's modified Eagle's medium (DMEM; Sigma-Aldrich, St. Louis, MO, USA) supplemented with 10% heat-inactivated fetal bovine serum (Life Technologies, Foster City, CA, USA) in a humidified atmosphere containing 5% CO_2 at 37°C.

For the splicing assay, COS-7 cells were cultured in 12-well plates and transfected with 0.1 μg of the *Clcn1* minigene and AONs (0.1 μmol) at 60–80% confluence. Polyethylenimine and Endo-Porter (Gene Tools) were used for the transfection of PS2OMe RNA and PMOs, respectively. Forty-eight hours later, total RNA was extracted from the transfected cells using a GenElute Mammalian Total RNA Miniprep Kit (Sigma-Aldrich).

Animals. HSA^{LR} mice are FVB/n-background transgenic mice that express expanded CTG repeats under the control of the human skeletal actin promoter in skeletal muscle[38]. Compared with the first established line, the number of the repeat was reduced: the mice used in this study carried 180–200 repeats. All the mutant mice showed persistent contraction of gluteal muscles after they bucked. We used FVB/nJcl mice (Clea Japan, Tokyo, Japan) as wild-type controls.

The present study was approved by the Ethical Committee for Animal Experiments at the University of Tokyo, and was carried out in accordance with the Guidelines for Research with Experimental Animals of the University of Tokyo and the NIH Guide for the Care and Use of Laboratory Animals (NIH Guide, revised 1996).

Bubble liposomes. Bubble liposomes were prepared by previously described methods[24]. Briefly, PEG liposomes composed of 1,2-dipalmitoyl-sn-glycero-3-phosphocholine (DPPC) (NOF Corporation, Tokyo, Japan) and 1,2-distearoyl-sn-glycero-3-phosphatidyl-ethanolamine-polyethyleneglycol (DSPE-PEG2000-OMe) (NOF Corporation) at a molar ratio of 94 : 6 were prepared by a reverse phase evaporation method. Briefly, all reagents were dissolved in 1 : 1 (v/v) chloroform/diisopropyl ether. Phosphate-buffered saline was added to the lipid solution, and the mixture was sonicated and then evaporated at 47°C. The organic solvent was completely removed, and the size of the liposomes was adjusted to less than 200 nm using extruding equipment and a sizing filter (pore size: 200 nm) (Nuclepore Track-Etch Membrane; Whatman Plc, Maidstone, Kent, UK). The lipid concentration was measured using a Phospholipid C test (Wako Pure Chemical Industries, Ltd, Osaka, Japan). Bubble liposomes were prepared from liposomes and perfluoropropane gas (Takachio Chemical Ind. Co. Ltd, Tokyo, Japan). First, 2-ml sterilised vials containing 0.8 ml of liposome suspension (lipid concentration: 1 mg/ml) were filled with perfluoropropane gas, capped and then pressurised with a further 3 ml of perfluoropropane gas. The vial was placed in a bath-type sonicator (38 kHz, 250 W) (SONO-CLEANER CA-4481L; Kaijo Denki, Tokyo, Japan) for 1 min to form Bubble liposomes.

Injection of morpholino oligonucleotides with Bubble liposomes and ultrasound. PMO (20 μg) and the Bubble liposome suspension (30 μl) were injected into the TA muscles of *HSA*^{LR} mice (6 weeks old) using a 30-gauge needle (NIPRO Co., Osaka, Japan). Immediately after injection, ultrasound (frequency, 1 MHz; duty, 50%; intensity, 2.0 W/cm^2; time, 60 s) was applied transdermally downstream of the injection site using a 6-mm diameter probe. A SONITRON 1000 device (Rich-Mar, Chattanooga, TN, USA) was used to generate the ultrasound. We administrated the PMO three times at weekly intervals. Three weeks after the last administration, we performed EMG measurements and then killed the mice and harvested the TA muscles for RT-PCR analysis and immunohistochemistry.

Electromyographic recording and electrical stimulation. Implantation of EMG electrodes and stimulating electrodes was carried out under aseptic conditions on mice anaesthetised with 2% vapourised isoflurane in air. Body temperature was measured rectally and was maintained at 37–38°C using a homeothermic heating pad (BioResearch Center, Aichi, Japan). Bipolar wire electrodes (tip distance, 1–2 mm) made of Teflon-insulated stainless steel wire (76 μm diameter bare, 140 μm coated; cat. no. 791000; A-M Systems, Carlsborg, WA, USA) were implanted in the TA and gastrocnemius (GA) muscles to record EMG activity. The electrical stimulation of the TA muscle was achieved using two wire electrodes that were inserted under the skin over the TA muscle and placed along the longitudinal axis of the muscle. After full recovery from the anaesthesia, alert mice were restrained in a cylindrical mouse-sized cage, with their hind limbs out of the cage to maintain their muscles at their resting lengths. The EMG signals were amplified and bandpass filtered (15 Hz–1 KHz; AB-611J; Nihon-Koden, Co., Tokyo, Japan), digitised with an analog-digital converter (PowerLab 16/30, ADInstruments Ltd, Oxford, UK) and recorded (sampling rate 10 kHz) on a computer. Electrical stimulation consisted of repetitive square pulses (train of 20 pulses at 100 Hz, 1 ms duration) delivered by an isolation unit (SS-202J; Nihon-Koden) connected to a pulse generator (SEN-3401, Nihon-Koden). The stimulus intensity was adjusted to evoke ankle dorsiflexion and avoid overt movements and animal discomfort. EMG measurements were recorded in single-blinded manner.

EMG data analysis. Myotonic EMG activities were easily confirmed by visual inspection and analysed using custom-written MATLAB software (MathWorks, Inc., Natick, MA, USA). EMG signals were full-wave-rectified and filtered with a 20 Hz low-pass second-order Butterworth filter. Offset of the EMG signal was defined as a deflection below three standard deviations from baseline. The baseline level was defined as the mean EMG signal in the resting state before stimulation. Duration of myotonic activities was defined as the period from the termination of stimulation to the offset time. Myotonic activities were integrated during the duration of myotonia and calculated by subtracting the baseline level. To quantify EMG activities per unit time, iEMG values were then calculated as the integrated myotonia value divided by corresponding net duration. The EMG data were analysed in a single-blinded manner.

RT-PCR analysis. Total RNA was extracted from TA muscles and cultured cells using TRIzol reagent (Life Technologies) and a GenElute Mammalian Total RNA Miniprep Kit (Sigma-Aldrich), respectively, according to the manufacturers' instructions.

Typically, 0.5–1.0 μg of total RNA was reverse-transcribed with a PrimeScript 1st Strand cDNA Synthesis Kit (Takara Bio, Shiga, Japan) using oligo(dT) primers. PCR reactions were performed using Ex Taq DNA polymerase (Takara Bio). The sequences of the PCR primers are listed in Supplementary Table ST2. The products were electrophoretically resolved on an 8% polyacrylamide gel that was stained with ethidium bromide and analysed using an LAS-3000 luminescence image analyser (FujiFilm, Tokyo, Japan). The ratio of exon 7A inclusion in *Clcn1* mRNA was calculated as (7A inclusion)/(7A inclusion + 7A skipping) × 100.

Immunofluorescence. Frozen sections (6 μm thick) of unfixed TA muscles were immunostained with an affinity-purified rabbit polyclonal anti-Clcn1 antibody (dilution 1 : 50; Alpha Diagnostics International, San Antonio, TX, USA). The secondary antibody was Alexa Fluor 488-conjugated goat anti-rabbit IgG (Life Technologies) used at a dilution of 1 : 600. Images were collected using an IX70 inverted microscope (Olympus, Tokyo, Japan) equipped with a ×20 objective lens. Exposure time and threshold were identical for all comparisons of antisense and saline controls.

Statistics. A two-tailed Student's *t*-test or Tukey's multiple comparison test were used for statistical comparison.

1. Aslanidis, C. *et al.* Cloning of the essential myotonic dystrophy region and mapping of the putative defect. *Nature* **355**, 548–551 (1992).
2. Brook, J. D. *et al.* Molecular basis of myotonic dystrophy: expansion of a trinucleotide (CTG) repeat at the 3′ end of a transcript encoding a protein kinase family member. *Cell* **68**, 799–808 (1992).
3. Buxton, J. *et al.* Detection of an unstable fragment of DNA specific to individuals with myotonic dystrophy. *Nature* **355**, 547–548 (1992).
4. Harley, H. G. *et al.* Expansion of an unstable DNA region and phenotypic variation in myotonic dystrophy. *Nature* **355**, 545–546 (1992).
5. Harper, P. S. *Myotonic dystrophy,* 3rd ed. (Saunders, W. B. Philadelphia, 2001).
6. Philips, A. V., Timchenko, L. T. & Cooper, T. A. Disruption of splicing regulated by a CUG-binding protein in myotonic dystrophy. *Science* **280**, 737–741 (1998).
7. Savkur, R. S., Philips, A. V. & Cooper, T. A. Aberrant regulation of insulin receptor alternative splicing is associated with insulin resistance in myotonic dystrophy. *Nat. Genet.* **29**, 40–47 (2001).
8. Fugier, C. *et al.* Misregulated alternative splicing of BIN1 is associated with T tubule alterations and muscle weakness in myotonic dystrophy. *Nat. Med.* **17**, 720–725 (2011).
9. Koebis, M. *et al.* Alternative splicing of myomesin 1 gene is aberrantly regulated in myotonic dystrophy type 1. *Genes Cells* **16**, 961–972 (2011).
10. Ohsawa, N., Koebis, M., Suo, S., Nishino, I. & Ishiura, S. Alternative splicing of PDLIM3/ALP, for alpha-actinin-associated LIM protein 3, is aberrant in persons with myotonic dystrophy. *Biochem. Biophys. Res. Commun.* **409**, 64–69 (2011).
11. Charlet, B. N. *et al.* Loss of the muscle-specific chloride channel in type 1 myotonic dystrophy due to misregulated alternative splicing. *Mol. Cell.* **10**, 45–53 (2002).
12. Mankodi, A. *et al.* Expanded CUG repeats trigger aberrant splicing of ClC-1 chloride channel pre-mRNA and hyperexcitability of skeletal muscle in myotonic dystrophy. *Mol. Cell.* **10**, 35–44 (2002).
13. Lossin, C. & George, A. L. Jr. Myotonia congenita. *Adv. Genet.* **63**, 25–55 (2008).
14. Wheeler, T. M., Lueck, J. D., Swanson, M. S., Dirksen, R. T. & Thornton, C. A. Correction of ClC-1 splicing eliminates chloride channelopathy and myotonia in mouse models of myotonic dystrophy. *J. Clin. Invest.* **117**, 3952–3957 (2007).
15. Kole, R., Krainer, A. R. & Altman, S. RNA therapeutics: beyond RNA interference and antisense oligonucleotides. *Nat. Rev. Drug. Discov.* **11**, 125–140 (2012).
16. Stein, D., Foster, E., Huang, S. B., Weller, D. & Summerton, J. A specificity comparison of four antisense types: morpholino, 2′-O-methyl RNA, DNA, and phosphorothioate DNA. *Antisense Nucleic Acid Drug Dev.* **7**, 151–157 (1997).
17. Wu, B. *et al.* Dose-dependent restoration of dystrophin expression in cardiac muscle of dystrophic mice by systemically delivered morpholino. *Gene Ther.* **17**, 132–140 (2010).
18. Wheeler, T. M. *et al.* Targeting nuclear RNA for in vivo correction of myotonic dystrophy. *Nature* **488**, 111–115 (2012).
19. Leger, A. J. *et al.* Systemic delivery of a peptide-linked morpholino oligonucleotide neutralizes mutant RNA toxicity in a mouse model of myotonic dystrophy. *Nucleic Acid Ther.* **23**, 109–117 (2013).
20. Lu, Q. L., Liang, H. D., Partridge, T. & Blomley, M. J. Microbubble ultrasound improves the efficiency of gene transduction in skeletal muscle in vivo with reduced tissue damage. *Gene Ther.* **10**, 396–405 (2003).
21. Shen, Z. P., Brayman, A. A., Chen, L. & Miao, C. H. Ultrasound with microbubbles enhances gene expression of plasmid DNA in the liver via intraportal delivery. *Gene Ther.* **15**, 1147–1155 (2008).
22. Haag, P. *et al.* Microbubble-enhanced ultrasound to deliver an antisense oligodeoxynucleotide targeting the human androgen receptor into prostate tumours. *J. Steroid Biochem. Mol. Biol.* **102**, 103–113 (2006).
23. Suzuki, R. *et al.* Gene delivery by combination of novel liposomal bubbles with perfluoropropane and ultrasound. *J. Control Release* **117**, 130–136 (2007).
24. Negishi, Y. *et al.* Delivery of an angiogenic gene into ischemic muscle by novel bubble liposomes followed by ultrasound exposure. *Pharm. Res.* **28**, 712–719 (2011).
25. Negishi, Y. *et al.* Local gene delivery system by bubble liposomes and ultrasound exposure into joint synovium. *J. Drug Deliv.* **2011**, 203986 (2011).
26. Negishi, Y. *et al.* Systemic delivery systems of angiogenic gene by novel bubble liposomes containing cationic lipid and ultrasound exposure. *Mol. Pharm.* **9**, 1834–1840 (2012).
27. Sugano, M. *et al.* Gene delivery system involving Bubble liposomes and ultrasound for the efficient in vivo delivery of genes into mouse tongue tissue. *Int. J. Pharm.* **422**, 332–337 (2012).
28. Negishi, Y. *et al.* AG73-modified Bubble liposomes for targeted ultrasound imaging of tumor neovasculature. *Biomaterials* **34**, 501–507 (2013).
29. Kino, Y. *et al.* MBNL and CELF proteins regulate alternative splicing of the skeletal muscle chloride channel CLCN1. *Nucleic Acids Res.* **37**, 6477–6490 (2009).
30. Lin, X. *et al.* Failure of MBNL1-dependent post-natal splicing transitions in myotonic dystrophy. *Hum. Mol. Genet.* **15**, 2087–2097 (2006).
31. Summerton, J. & Weller, D. Morpholino antisense oligomers: design, preparation, and properties. *Antisense Nucleic Acid Drug Dev.* **7**, 187–195 (1997).
32. Templeton, N. S. & Templeton, N. S. *Gene and cell therapy: therapeutic mechanisms and strategies.* 2nd ed. (Marcel Dekker, New York, 2004).
33. Sazani, P. *et al.* Systemically delivered antisense oligomers upregulate gene expression in mouse tissues. *Nat. Biotechnol.* **20**, 1228–1233 (2002).
34. Chen, M. F., Niggeweg, R., Iaizzo, P. A., Lehmann-Horn, F. & Jockusch, H. Chloride conductance in mouse muscle is subject to post-transcriptional compensation of the functional Cl- channel 1 gene dosage. *J. Physiol.* **504**, 75–81 (1997).
35. Berg, J., Jiang, H., Thornton, C. A. & Cannon, S. C. Truncated ClC-1 mRNA in myotonic dystrophy exerts a dominant-negative effect on the Cl current. *Neurology* **63**, 2371–2375 (2004).
36. Ranum, L. P. & Cooper, T. A. RNA-mediated neuromuscular disorders. *Annu. Rev. Neurosci.* **29**, 259–277 (2006).

37. Wheeler, T. M. *et al.* Reversal of RNA dominance by displacement of protein sequestered on triplet repeat RNA. *Science* **325**, 336–339 (2009).
38. Mankodi, A. *et al.* Myotonic dystrophy in transgenic mice expressing an expanded CUG repeat. *Science* **289**, 1769–1773 (2000).

Acknowledgements

We thank Prof. Charles A. Thornton (University of Rochester) for providing us *HSA*^{LR} mice. We also thank Dr H. Mitsuhashi for valuable discussions and encouragement. This work was supported in part by the Comprehensive Research on Disability Health and Welfare, from the Ministry of Health, Labour and Welfare Japan, and Intramural Research Grant (23–5) for Neurological and Psychiatric Disorders of NCNP.

Author contributions

S.I. conceived the project. M.K. designed the experiments. T.K. carried out cell culture-based splicing assay. K.N., M.P.T. carried out the delivery of PMO. R.M., Y.H. and I.N. carried out histochemical staining. H.Y., M.H., M.S. and D.Y. designed and carried out EMG analysis. Y.N. and Y.E.-T. prepared Bubble liposomes.

Additional information

Supplementary Information accompanies this paper at http://www.nature.com/scientificreports

Competing financial interests: The authors declare no competing financial interests.

How to cite this article: Koebis, M. *et al.* Ultrasound-enhanced delivery of Morpholino with Bubble liposomes ameliorates the myotonia of myotonic dystrophy model mice. *Sci. Rep.* **3**, 2242; DOI:10.1038/srep02242 (2013).

SCIENTIFIC REPORTS

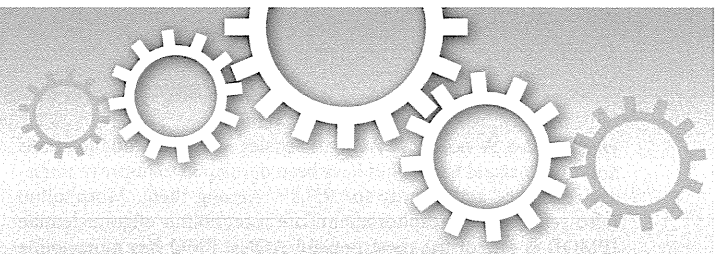

OPEN

SUBJECT AREAS:
MECHANISMS OF DISEASE
ANTISENSE OLIGO
DRUG DELIVERY
RNA SPLICING

Received
18 March 2013

Accepted
21 June 2013

Published
22 July 2013

Correspondence and requests for materials should be addressed to S.I. (cishiura@mail.ecc.u-tokyo.ac.jp)

Ultrasound-enhanced delivery of Morpholino with Bubble liposomes ameliorates the myotonia of myotonic dystrophy model mice

Michinori Koebis[1], Tamami Kiyatake[1], Hiroshi Yamaura[1], Kanako Nagano[1], Mana Higashihara[2], Masahiro Sonoo[3], Yukiko Hayashi[4], Yoichi Negishi[5], Yoko Endo-Takahashi[5], Dai Yanagihara[1], Ryoichi Matsuda[1], Masanori P. Takahashi[6], Ichizo Nishino[4] & Shoichi Ishiura[1]

[1]Graduate School of Arts and Sciences, the University of Tokyo, Tokyo, Japan, [2]Division of Neurology, Department of Internal Medicine 3, National Defense Medical College, Saitama, Japan, [3]Department of Neurology, Teikyo University School of Medicine, Tokyo, Japan, [4]Department of Neuromuscular Research, National Institute of Neuroscience, National Center of Neurology and Psychiatry (NCNP), Tokyo, Japan, [5]Department of Drug Delivery and Molecular Biopharmaceutics, School of Pharmacy, Tokyo University of Pharmacy and Life Sciences, Tokyo, Japan, [6]Department of Neurology, Osaka University Graduate School of Medicine, Osaka, Japan.

Phosphorodiamidate morpholino oligonucleotide (PMO)-mediated control of the alternative splicing of the chloride channel 1 (*CLCN1*) gene is a promising treatment for myotonic dystrophy type 1 (DM1) because the abnormal splicing of this gene causes myotonia in patients with DM1. In this study, we optimised a PMO sequence to correct *Clcn1* alternative splicing and successfully remedied the myotonic phenotype of a DM1 mouse model, the HSA^{LR} mouse. To enhance the efficiency of delivery of PMO into HSA^{LR} mouse muscles, Bubble liposomes, which have been used as a gene delivery tool, were applied with ultrasound exposure. Effective delivery of PMO led to increased expression of Clcn1 protein in skeletal muscle and the amelioration of myotonia. Thus, PMO-mediated control of the alternative splicing of the *Clcn1* gene must be important target of antisense therapy of DM1.

Myotonic dystrophy type 1 (DM1) is caused by expansion of the CTG repeat in the 3′ untranslated region (UTR) of the *DMPK* gene[1–4]. Patients with DM1 show multi-systemic symptoms, including muscle wasting, muscle weakness, myotonia, cardiac conduction defect, cataracts, mental retardation and insulin resistance[5]. A patient, however, does not always present with all of these symptoms and the severity of the disease varies among individuals. Among the symptoms, myotonia is the most prominent and common phenotype of DM1: most patients feel muscle stiffness and difficulty in relaxing muscles soon after developing the disease.

The characteristic feature of the pathology of DM1 is the aberrant regulation of dozens of alternative splicing events, and some of the abnormal splicing events have been suggested to be involved in some of the symptoms[6–10]. Myotonic discharge is thought to be caused by the aberrant alternative splicing of the chloride channel 1 (*CLCN1*) gene[11,12]. In patients with DM1, extra exons from intron 6 are spliced into the *CLCN1* mRNA, leading to the appearance of a premature termination codon in the subsequent exon, degradation of the mRNA by nonsense-mediated decay and decreased expression of CLCN1 protein[11]. The idea that abnormal splicing of the *CLCN1* gene causes myotonia is strongly supported by the fact that the *CLCN1* gene is the only gene responsible for congenital myotonia, and the identification of multiple mutations in patients with the disease and their families[13]. Wheeler and his colleagues corrected the abnormal splicing of the *Clcn1* gene in a DM1 mouse model, the HSA^{LR} mouse, by using an antisense oligonucleotide (AON) and successfully alleviated the myotonic phenotype[14]. Thus, correction of the abnormally regulated splicing is a promising treatment for DM1.

An AON is a short, synthetic nucleic acid molecule with a sequence complementary to a target transcript. It can be used to manipulate an alternative splicing event: the AON that binds to the region around the target exon, specifically splice sites or splicing enhancer domains, physically blocks assembly of the spliceosome on the exon and induces exon skipping[15]. The efficacy of an AON is dependent on its half-life, affinity for its target RNA and *in*

vivo kinetics. A variety of AON molecules with 2′-*O* modifications and/or unnatural backbones have been developed to improve nuclease resistance and affinity for RNA[15]. Among them, Morpholino (also referred as phosphorodiamidate morpholino oligonucleotide [PMO]) is one of the most hopeful AONs. PMO has morpholine rings linked with phosphorodiamidate linkages in its backbone instead of deoxyribose and phosphodiester bonds. Due to its completely unnatural chemistry, PMO is hardly recognised by cellular nucleases. It has higher affinity for RNA than for DNA; the T_m value of a hybrid of PMO and RNA is much higher than that of DNA and RNA[16]. Several papers have reported the local and systemic administration of PMO to mice and dogs. For example, when a high dose of PMO (3 g/kg) was administrated intravenously into the *mdx* mouse, a mouse model of Duchenne muscular dystrophy, the PMO entered skeletal muscle without any assistive delivery reagent[17]. However, unlike mdx mice, muscle penetration of Evans Blue dye did not increase in HSA^{LR} and wild-type mice[18], which indicated a physical barrier to PMO uptake should be grater in HSA^{LR} than in *mdx*. In preceding reports on PMO treatment in HSA^{LR}, intravenous administration of CAG25 PMO led no detectable improvements in *Serca1* splicing in HSA^{LR} mice[19], and even when PMO was injected intramuscularly its uptake was limited to the needle track[14]. In these studies, they used electroporation to administer unmodified PMO intramuscularly, so we investigated a less invasive PMO delivery method to develop PMO treatment for DM1.

Recently, ultrasound exposure has been used for the intracellular delivery of molecules such as dextran, plasmid DNA and siRNA. If ultrasound is sufficiently strong, it will generate microscopic vacuum bubbles in a solution by a process known as inertial cavitation. The bubbles immediately collapse, producing a shock wave, which is believed to transiently increase the permeability of cell membranes in the vicinity. Inertial cavitation is enhanced by using micro bubbles of echo-contrast gas. This method has been applied to gene delivery into various mouse tissues, including skeletal muscle, liver and tumour tissues[20–22]; however, introducing genes into deep tissues with microbubbles is difficult because of their size and instability. To overcome these problems, we previously developed a novel drug delivery reagent coined "Bubble liposomes", polyethylene glycol-modified liposomes (PEG liposomes) encapsulating echo-contrast gas[23]. Owing to the stability in serum and uniform microscopic size of PEG liposomes, we successfully delivered genes and siRNA into several tissues[24–28]. However, does the Bubble liposome-ultrasound delivery system efficiently deliver PMO into skeletal muscles in the HSA^{LR} mice? In this study, we examined the ability of the Bubble liposome-ultrasound system to deliver PMO into skeletal muscles of HSA^{LR} mice as a treatment for abnormal splicing.

We newly designed antisense PMOs targeting exon 7A of the *Clcn1* gene and delivered them into HSA^{LR} mice. The PMOs were successfully delivered into skeletal muscles by the Bubble liposome-ultrasound system, which decreased the inclusion of exon 7A *in vivo*. Furthermore, the injection of PMO ameliorated the myotonic phenotype of the model mice. Our results suggest that Bubble liposomes should be effective for delivering PMOs into muscle tissues and can be applied to PMO treatment of DM1.

Results

We first determined the optimal target sequence of the *Clcn1* pre-mRNA to promote skipping of exon 7A. To achieve this, we used a *Clcn1* minigene and examined its alternative splicing using a cell culture-based assay. The minigene contains the genomic region from exon 6 to exon 7 of the murine *Clcn1* gene. When it was transfected into COS-7 cells, approximately 50% of transcripts contained exon 7A (Fig. 1b, minigene only). To screen for an optimal AON sequence, we used 25-mer phosphorothioate 2′ *O*-methyl (PS2OMe) RNA, which can regulate alternative splicing by sterically preventing spliceosomal assembly, just like PMO. We examined PS2OMe RNA molecules that covered the whole of exon 7A (1–25, 26–50, 51–75 and 76–90) and the boundary of intron 6 and exon 7A (−10–15). We transfected the minigene together with the PS2OMe RNA into COS-7 cells and analysed the alternative splicing of the minigene. We found that −10–15 and 1–25 PS2OMe significantly reduced the rate of inclusion of exon 7A, with 1–25 PS2OMe being the most effective molecule (Fig. 1b).

Previously, we identified the 8 nt at the 5′ end of exon 7A as an exonic splicing enhancer (ESE) essential for basal inclusion of the exon[29]. Given that both −10–15 and 1–25 PS2OMe covered the ESE, and that 1–25 PS2OMe seemed to be more effective at excluding exon 7A, we speculated that another ESE (16–25) would be located in the region +16 to +25, and that 1–25 PS2OMe would not share it with −10–15 PS2OMe. To examine this possibility, we tested whether 16–40 PS2OMe enhanced normal splicing. 16–40 PS2OMe markedly reduced the rate of inclusion of exon 7A of the *Clcn1* minigene (Supplementary Fig. S1). As 26–50 PS2OMe did not change the alternative splicing, we conclude that the other ESE (16–25) is important for exon 7A inclusion. Thus, we used 1–25 AON, which targeted both ESEs, in subsequent experiments.

PS2OMe is highly resistant to nuclease-mediated degradation owing to its phosphorothioate linkages; however, it is still degraded slowly and releases monomers that have a toxic, free phosphorothioate group. In contrast, PMO is remarkably resistant to degradation and is not noxious. Therefore, we next investigated whether a PMO with the same sequence as 1–25 PS2OMe also improved the alternative splicing of exon 7A by using the cell culture-based splicing assay (Fig. 1c). The −11–14 PMO we used here had the same sequence as that Wheeler and his colleagues used in a previous study[14]. RT-PCR analysis showed that both 1–25 and −11–14 PMOs significantly reduced exon 7A inclusion. Although the effect of 1–25 PMO was greater than that of −11–14 PMO, no statistically significant difference was observed between them.

1–25 PMO was so effective at improving alternative splicing of the *Clcn1* minigene in cultured cells that we expected it to work well *in vivo*. To test whether 1–25 PMO could work *in vivo*, we administrated 60 μg of 1–25 PMO intramuscularly four times at weekly intervals into the *tibialis anterior* (TA) muscles of HSA^{LR} mice. The alternative splicing of the *Clcn1* gene was moderately improved, with an approximately 30% decrease in exon 7A inclusion. Electromyography (EMG) with a single needle electrode, however, revealed that the occurrence of myotonia was not altered by PMO injection (Supplementary Fig. S2). Because 60 μg of PMO was quite a high dose for administration into a single muscle, we assumed that an effective delivery system would be required to introduce 1–25 PMO into muscle tissues. We therefore examined the usefulness of ultrasound-enhanced delivery with Bubble liposomes for PMO delivery. We administrated 20 μg of 1–25 PMO three times at weekly intervals into the TA muscles of HSA^{LR} mice with or without Bubble liposomes and ultrasound (Fig. 2). RT-PCR analysis revealed that the rate of inclusion of exon 7A decreased to its lowest level when both Bubble liposomes and ultrasound were applied, indicating that use of the combination of Bubble liposomes and ultrasound could enhance PMO delivery efficiency.

We next investigated whether 1–25 PMO could cure myotonic symptoms in HSA^{LR} mice when delivered using the Bubble liposome-ultrasound system. We administrated 1–25 PMO as described above. Three weeks later, we harvested the injected muscles and conducted RT-PCR and immunohistological analyses. RT-PCR showed that 1–25 PMO decreased the inclusion of exon 7A to a level comparable to that in wild-type FVB/n mice (Fig. 3a). We checked four other alternative splicing events, *Cypher* (*Ldb3*) exon 11, *Mbnl1* exon 5, *Ryr1* exon 70 and *Serca1* exon 22, which are known to be abnormally regulated in patients with DM1and HSA^{LR} mice[30]. We found that the alternative splicing of none of them was changed by

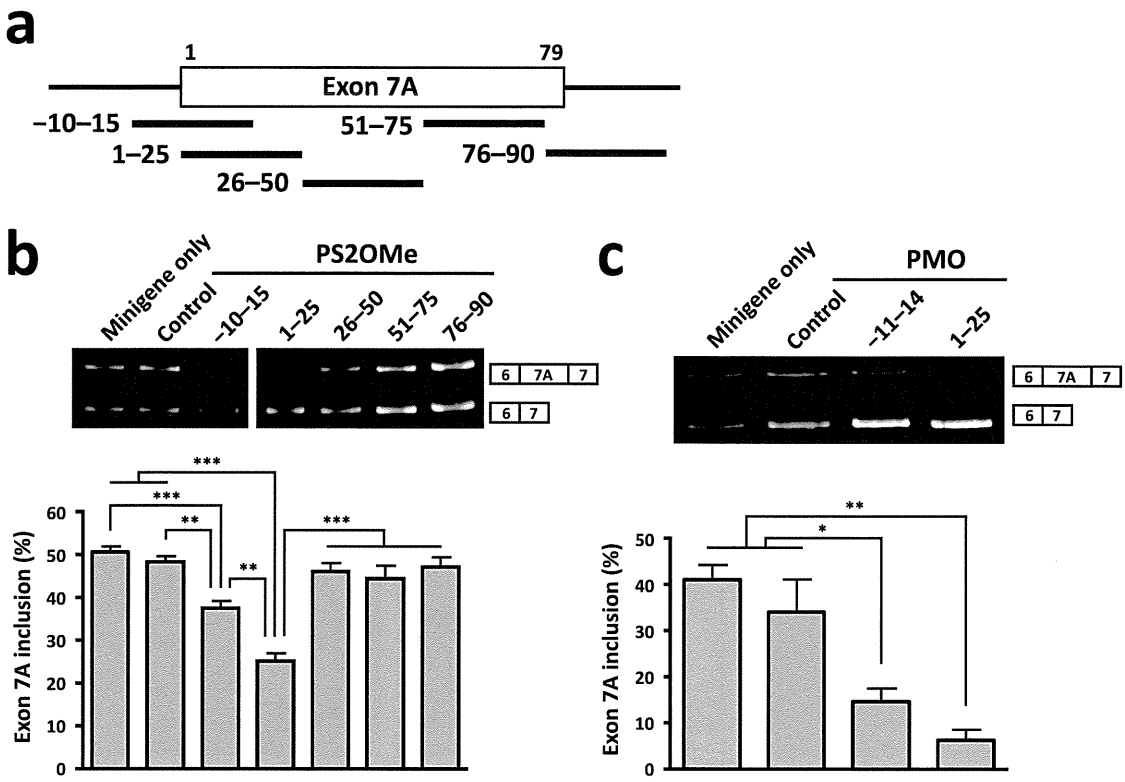

Figure 1 | AON-mediated exclusion of *Clcn1* exon 7A in COS-7 cells. (a) Locations of the target sites of AONs (thick black lines) along the *Clcn1* pre-mRNA. The numbers over exon 7A (rectangle) indicate the positions of nucleotides. (b) Cellular splicing assay to detect the exclusion of exon 7A of the *Clcn1* minigene by PS2OMe RNA in COS-7 cells. 1–25 was the most successful AON. A representative result is shown above and the bars indicate mean and s.e.m. ($n = 6$). (c) The same assay as in (b) except that PMOs were used. 1–25 PMO decreased the inclusion of exon 7A effectively ($n = 3$). Statistical significance was analysed by Tukey's multi-comparison test (* $P < 0.05$, ** $P < 0.01$, *** $P < 0.001$).

the injection of 1–25 PMO (Fig. 3b); thus, the effect of the PMO was specific to the alternative splicing of the *Clcn1* gene.

The abnormal splicing of *Clcn1* is believed to cause myotonia by introducing a premature termination codon into the subsequent exon and by decreasing the expression of the Clcn1 protein via nonsense-mediated mRNA decay. Thus, we examined whether 1–25 PMO restored the expression of Clcn1 protein in HSA^{LR} mice. Immunofluorescence analysis of TA muscles showed the sarcolemmal localisation of Clcn1 protein in wild-type muscle, but such a pattern was not detected in saline-injected HSA^{LR} mice. The injection of 1–25 PMO clearly restored the sarcolemmal distribution, demonstrating that correction of the abnormal splicing of the *Clcn1* gene led to the normal expression of its protein (Fig. 3c).

Finally, we investigated whether injection of 1–25 PMO improved the myotonic phenotype of HSA^{LR} mice. Electromyographic analyses showed bursts of action potentials after electrical stimulation (4–8 V) in HSA^{LR} mice, but not in wild-type mice (Fig. 4a). Myotonia occurred even in denervated muscles (data not shown), which indicates that it was not caused by hyperactivation of motor neurones, but by increased excitability of the sarcolemma. Myotonic EMG activities continued for 1 to 3 s and their average duration was 1.27 s in saline-treated TA muscles. The injection of 1–25 PMO decreased their duration, but the change was not statistically significant; the integrated EMG (iEMG) was reduced by the PMO administration ($P < 0.05$). The decreased iEMG indicated that 1–25 PMO mitigated the hyperexcitability of the HSA^{LR} muscles.

These results suggest that 1–25 PMO could improve the function of the *Clcn1* gene in the DM1 model mouse at the RNA, protein and

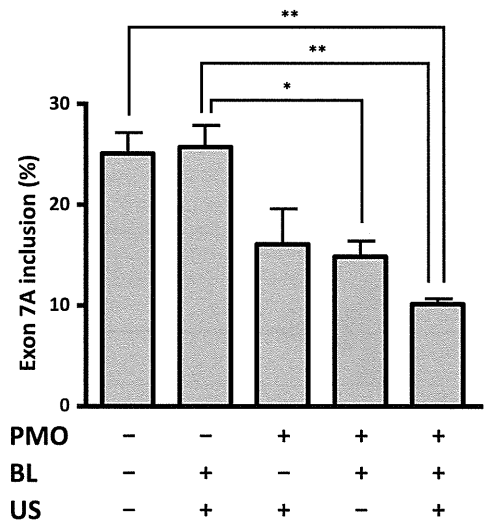

Figure 2 | PMO delivery by the combination of Bubble liposomes and ultrasound. 1–25 PMO (20 μg) or saline was locally administrated into TA muscles of HSA^{LR} mice with/without Bubble liposomes (BLs) and ultrasound (US). The inclusion rate of exon 7A decreased most when both Bubble liposomes and ultrasound were applied. ($n = 3$). The bars indicate mean and s.e.m., and statistical significance was analysed by Tukey's multi-comparison test (* $P < 0.05$, ** $P < 0.01$).